Graduate School ETD Form 9
(Revised 01/14)

PURDUE UNIVERSITY
GRADUATE SCHOOL
Thesis/Dissertation Acceptance

This is to certify that the thesis/dissertation prepared

By Wen Chao Lee

Entitled
A NEW CHEMICAL SYNTHESIS FOR VANADIUM SULFIDE AS HIGH PERFORMANCE CATHODE

For the degree of Master of Science in Mechanical Engineering

Is approved by the final examining committee:

Likun Zhu

El- Mounayri, Hazim A.

Jing Zhang

To the best of my knowledge and as understood by the student in the *Thesis/Dissertation Agreement. Publication Delay, and Certification/Disclaimer (Graduate School Form 32)*, this thesis/dissertation adheres to the provisions of Purdue University's "Policy on Integrity in Research" and the use of copyrighted material.

Likun Zhu

Approved by Major Professor(s): _____

Approved by: Sohel Anwar 04/29/2014

Head of the Department Graduate Program Date

A NEW CHEMICAL SYNTHESIS FOR VANADIUM SULFIDE AS HIGH PERFORMANCE CATHODE

A Thesis

Submitted to the Faculty

of

Purdue University

by

Wen Chao Lee

In Partial Fulfillment of the

Requirements for the Degree

of

Master of Science in Mechanical Engineering

May 2014

Purdue University

Indianapolis, Indiana

ACKNOWLEDGEMENTS

I would like to express my greatest gratitude to my advisor, Dr. Likun Zhu, for his supervision, guidance and financial assistance throughout my study in the Master's degree program. Dr. Zhu shared with me his knowledge and research experience even in my hardest time, for which I am always thankful.

I would like to thank my thesis committee members Dr. Hazim El-Mounayri and Dr. Jing Zhang for their time and participation in my thesis defense. Their advice and comments have further enriched the quality of this thesis. In addition, I extend thanks to Ms. Valerie Lim Diemer for assisting me with formatting my thesis.

Finally, and most importantly, will be my thanks and gratitude to my previous advisor, Dr. Youngsik Kim. Although he was my advisor for few months before he left to South Korea, I am very thankful for his guidance and knowledge on Li-ion battery field. I spent 2 years working on battery research with Dr. Kim, and I learnt a lot from him in term of academic and social life. I would also like stretch out my thanks to my friends who inspired me in this journey.

TABLE OF CONTENTS

Page

Page

LIST OF TABLES

LIST OF FIGURES

Figure Page

Figure Page

Figure Page

ABSTRACT

Lee, Wen Chao. M.S.M.E., Purdue University, May 2014. A New Chemical Synthesis for Vanadium Sulfide as High Performance Cathode. Major Professor: Likun Zhu.

Since 1990s, rechargeable Li-ion batteries have been widely used in consumer electronics such as cell phones, global positioning systems (GPS), personnel digital assistants (PDA), digital cameras, and laptop computers. Recently Li-ion batteries received considerable attention as a major power source for electric vehicles. However, significant technical challenges still exist for widely deploying Li-ion batteries in electric vehicles. For instance, the energy density of Li-ion batteries is not high enough to support a long-distance commute. The Li-ion batteries used for the Nissan Leaf and Chevy Volt only can support 50 – 100 miles per charge. The cost of Li-ion battery packs in electric vehicles is still high. The battery pack for the Chevy Volt costs about $8,000, and the larger one in the Nissan Leaf costs about $12,000. To address these problems, new Li-ion battery electrode materials with high energy density and low cost should be developed. Among Li-ion battery cathode materials, vanadium pentoxide, V_2O_5, is one of the earliest oxides studied as a cathode for Li-ion batteries because of its low cost, abundance, easy synthesis, and high energy density. However, its practical reversible capacity has been limited due to its irreversible structural change when Li insertion is more than $x = 1$.

Tremendous efforts have been made over the last twenty years to improve the phase reversibility of $Li_xV_2O_5$ (*e.g.*, $0 \leq x \leq 2$) because of vanadium pentoxides' potential use as high capacity cathodes in Li-ion batteries. In this thesis, a new strategy was studied to develop vanadium pentoxide cathode materials with improved phase reversibility. The first study is to synthesize vanadium oxide cathodes via a new chemical route – creating a

phase transformation from the vanadium sulfide to oxide. The β-$Na_{0.33}V_2O_5$ was prepared via a new method of chemical synthesis, involving the chemical transformation of $NaVS_2$ via heat-treatment at 600 °C in atmospheric air. The β-$Na_{0.33}V_2O_5$ particles were well crystalized and rod-shaped, measuring 7–15 μm long and 1–3 μm wide with the formation of the crystal defects on the surface of the particles. In contrast to previous reports contained in the literature, Na ions were extracted, without any structural collapse, from the β -$Na_{0.33}V_2O_5$ structure and replaced with Li ions during cycling of the cell in the voltage range, 1.5 V to 4.5 V. This eventually resulted in a fully reversible Li intercalation into the $Li_xV_2O_5$ structure when $0.0 \leq x \leq 2.0$.

The second study is to apply the synthesis method to $LiVS_2$ for the synthesis of β′-$Li_xV_2O_5$ for use as a high performance cathode. The synthesis method is based on the heat treatment of the pure $LiVS_2$ in atmospheric air. By employing this method of synthesis, well-crystalized, rod-shaped β′-$Li_xV_2O_5$ particles 20 – 30 μm in length and 3 – 6 μm in width were obtained. Moreover, the surface of β′-$Li_xV_2O_5$ particles was found to be coated by an amorphous vanadium oxysulfide film (~20 nm in thickness). In contrast to a low temperature vanadium pentoxide phase ($Li_xV_2O_5$), the electrochemical intercalation of lithium into the β′-$Li_xV_2O_5$ was fully reversible where $0.0 < x < 2.0$, and it delivered a capacity of 310 mAh/g at a current rate of 0.07 C between 1.5 V and 4 V. Good capacity retention of more than 88% was also observed after 50 cycles even at a higher current rate of 2 C.

The third study is the investigation of $NaVS_2$ as a cathode intercalation material for sodium ion batteries. We have shown that reversible electrochemical deintercalation of x ~ 1.0 Na per formula unit of Na_xVS_2, corresponding to a capacity of ~200 mAh/g, is possible. And a stable capacity of ~120 mAh/g after 30 cycles was observed.

These studies show that the new chemical synthesis route for creating a phase transformation from the vanadium sulfide to oxide by heat treatment in air is a promising method for preparing vanadium oxide cathode material with high reversibility. Although

this sample shows a relatively low voltage range compared with other cathodes such as $LiCoO_2$ (3.8 V) and $LiFePO_4$ (3.4 V), the large capacity of this sample is quite attractive in terms of increasing energy density in Li-ion batteries. Also, $NaVS_2$ could be a promising cathode material for sodium ion batteries.

CHAPTER 1. INTRODUCTION

1.1 Introduction

Fossil fuels, such as coal, petroleum, and natural gas have been the primary energy sources for modern society for many years. With the advancement of science and technolgy, the demond for energies has been increased significantly. Fossil fuels are non-renewable energy resources, which means they will eventually be depleted. Other than the conservation issue, environmental problems arising from a reliance on fossil fuels are becoming more and more severe, such as the air pollution in China in recent years. Moreover, the cost of fossil fuel has been increasing significant over the decades mainly due to decreasing resources over the world. One solution to address the energy and environmental problems is to replace fossil fuel with renewable energy sources. Aggressive research into alternative energy resources such as wind power, wave power , and solar power have been carried out [1]. The electrical energy produed from renewable energy resources could be stored and used for either stationary or mobile applications, such as electrical vehicles.

To store electrical energy, a suitable device is required. Therefore, researchers have been designing or inventing devices with the ability to store such renewable and eco-friendly energy. Energy can neither be created nor be destroyed, but it can be converted from one form to another form. Battery is a device that converts chemical energy to electrical energy. This device uses an electrochemical power source which utilizes the chemical reactions between chemical energy and electrical energy. Batteries are known for their high energy efficiency and do not produce harmful gases. There are many types of batteries, but the most famous or widely used batteries are Li-ion batteries. This

battery is rechargeable and has high energy density and low self-discharge rates compared to the others [2].

Li-ion batteries are widely used in portable electronic devices from cell phones to laptop compters, and even artificial body organs. Recently, Li-ion batteries have been used in electric vehicles (EVs) and hybrid electric vehicles (HEVs), such as Nissan Leaf and Chevy Volt. This is due to the high energy density, high power density, light weight and rechargeable properties of Li-ion batteries. Sony Corporation was the first company that manufactured the first commercialized Li-ion battery in the 1990s [3]. The demand for Li-ion batteries increased significantly throughout the years. However, one of the challenges that Li-ion batteries technology is facing now is due to the low capacity cathode compared to its anode [4].

In order to increase the specific capacity of Li-ion batteries, material selection is important; the material must have high voltage and high capacity properties. Alternative cathode material has been developed to increase the performance of Li-ion batteries. In this thesis, a new chemical route was investigated to develop a high capacity cathode material that can contribute to the further development of Li-ion battery technology.

The first chapter focuses on the literature review and some introduction to batteries. The main focus is on the concept of rechargeable Li-ion batteries and their operation principles. The components of these cells are described relatively. Furthermore, the attempts for developing new cathode and improving the existing cathode are discussed.

The second chapter of this thesis is focused on preparation of $NaVS_2$ using new chemical synthesis. The β-$Na_{0.33}V_2O_5$ was prepared via a new method of chemical synthesis, involving the chemical transformation of $NaVS_2$ via heat-treatment at 600 ℃ in atmospheric air. A variety of experments were carried out to investigate the performance of β-$Na_{0.33}V_2O_5$.

The third chapter will be discussing about structural effect on high performance cathode $LiVS_2$. The high temperature vanadium pentoxide phase, β'-$Li_xV_2O_5$, was synthesized via a new chemical synthesis involving the evolution of vanadium oxides from the 600 ℃ heat treatment of the pure $LiVS_2$ in air. The performance of β'-$Li_xV_2O_5$ were also investigated and discussed.

The forth chapter of this thesis is focused on reversible $NaVS_2$ (De)Intercalation Cathode for Na-Ion battery. We report for the first time the room-temperature insertion/extraction of Na from $NaVS_2$ in order to evaluate the feasibility of the material as a cathode for Na-ion batteries. The structural change of Na_xVS_2 is monitored as a function of Na content, and the stable room-temperature phase of $NaVS_2$ is determined.

The fifth chapter is about conclusions and future work.

1.2 Electrochemical Principles of Cells

In electrochemical cells, electrochemical reactions happen on the electrodes. Oxidation reaction happens on the anode side and reduction reaction happens on the cathode side. Electrons flow from the anode to the cathode during discharging process Anion also known as negative ions, flow from the cathode to anode through an electrolyte medium. Cation also known as positive ion, flow from the anode to the cathode through the electrolyte medium. On the cathode side, the reduction reaction occurs, represented by the following equation:

$$C + ne^- \rightleftharpoons C^{n-}$$

n : number of electrons received by material C

On the other hand, oxidation reaction occurs on the anode side of the cell, represented by the equation:

$$A \rightleftharpoons A^{n+} + ne^{-}$$

n : number of electrons lost from material A

The overall equation of the cell formed when the two half reactions are combined:

$$A + C \rightleftharpoons A^{n+} + C^{n-}$$

During the charging process, the negative electrode undergoes a reduction process, and the positive electrode undergoes an oxidation process. Conversely, the flow of electrons is reverse from cathode to anode. From the equation above, the reaction takes place in the backward direction. The operation of a cell during charging and discharging is shown schematically in Figure 1.1.

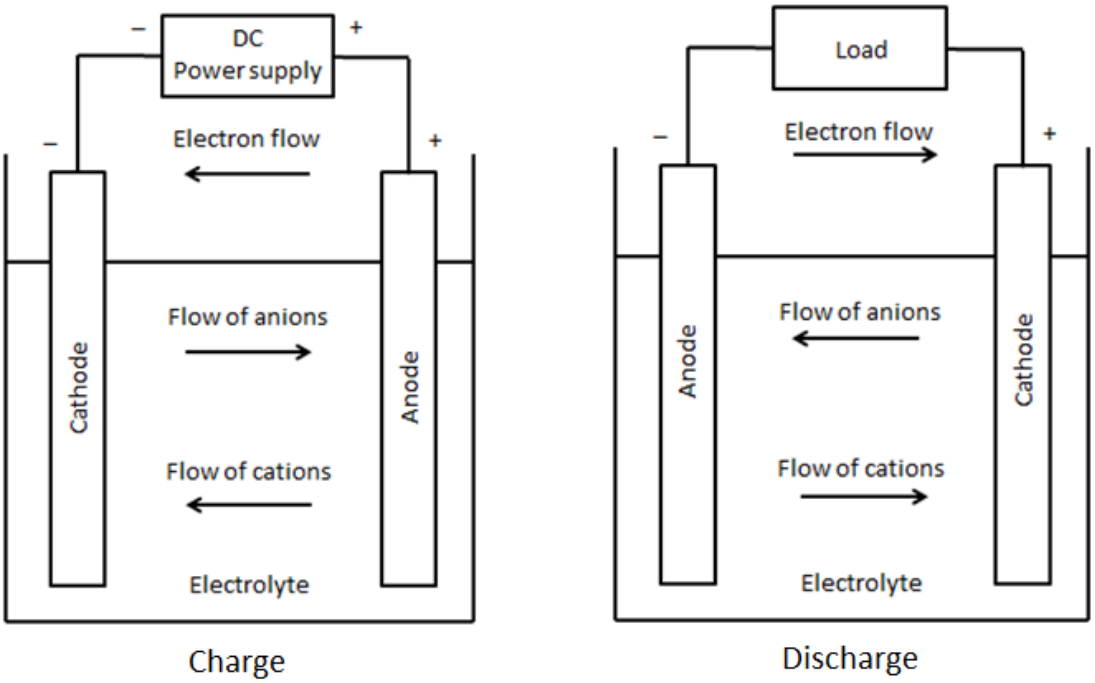

Figure 1.1 Electrochemical reaction of a cell during charging and discharging [1]

During the discharge process, the chemical energy of the active material is converted to the electrical energy. The potential of a galvanic cell is determined by Gibbs free energy of the chemical reaction inside the cell under standard conditions. The following equation shows the standard potential of a cell in terms of free energy of the system :

$$E° = -\frac{\Delta G°}{nF}$$

$\Delta G°$ = standard Gibbs energy of the reaction

n = number of electrons involved in the reaction

F = constant Faraday number ($\approx 96500C \; or \; 26.8Ah$)

$E°$ = standard potential of the cell.

Under non-standard conditions in terms of pressure, concentration and temperature, represented by the overall reaction below:

$$aA + bB \rightarrow cC + dD$$

The voltage of the cell is determined by the Nernst equation:

$$E = E° - \frac{RT}{nF} \ln \frac{C^c D^d}{A^a B^b}$$

R = gas constant,

T = absolute temperature, and

A, B, C, and D = activity of reactants and products

During the discharge process, the chemical energy from the battery will be converted into electrical energy. Battery cells are not 100% efficient. Internal impedances of the cell and polarization losses need to be taken into account when a load is applied to the cell. There are 2 types of polarization losses which are concentration and activation polarization. Concentration polarization occurs when there is a difference in the concentration of the surface of electrode. Activation polarization occurs when energy is required to overcome the energy barrier of the reaction.

Internal resistance also causes cell potential loss and reduces the performance of battery cell. The factors that affect internal resistance are resistance of materials, ionic conductivity of electrolytes, and contact resistance of current collectors and electrodes. In order to maintain the Ohm's law, the potential of the cell will drop to preserve the current. The governing equation for the operation voltage and external load R can be expressed as:

$$E = E_{\circ} - [(\eta_{ct})_a + (\eta_c)_a] - [(\eta_{ct})_c + (\eta_c)_c] - iR_i = iR$$

$E_{\circ}$ = the open circuit of the cell

$(\eta_{ct})_a, (\eta_{ct})_c$ = activation polarization at anode and cathode

$(\eta_c)_a, (\eta_c)_c$ = concentration polarization at anode and cathode

i = operating current of cell on load

R_i = internal resistance of the cell.

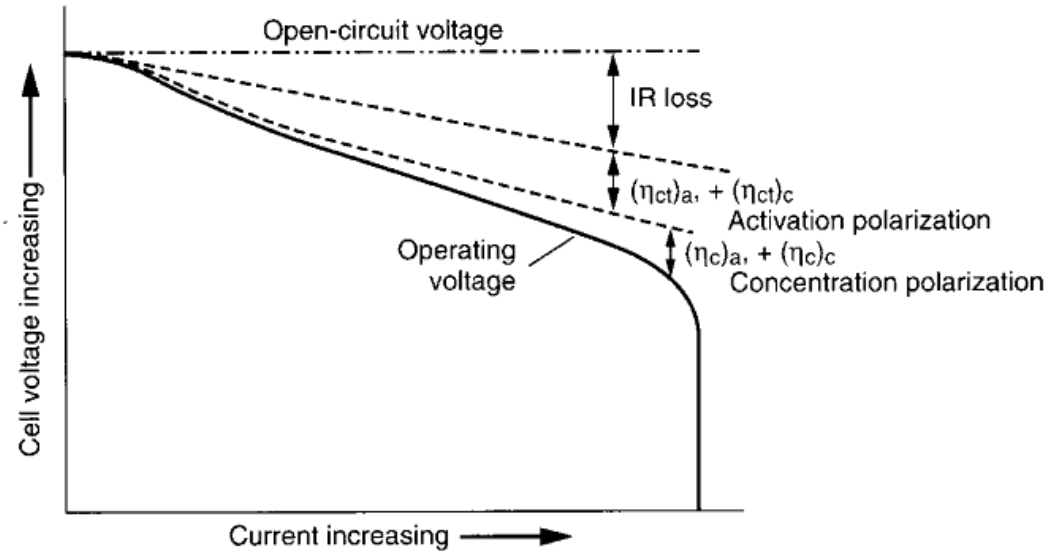

Figure 1.2 Voltage variations as a function of operating current due to the cell polarization [1]

1.3 Classification of Cells

Batteries can be categorized to primary and secondary batteries. The difference between them is that primary batteries are not able to recharge electrically and to be discarded after being used, while secondary batteries are capable of recharging

electrically multiple times. The secondary batteries are also known as “rechargeable batteries”.

1.3.1 Primary Batteries

Primary batteries have been used and studied for decades. Of all types of batteries, zinc-carbon battery with capacity of 50 Wh/kg was one of the first commercialized cells in 1940. Up to now, the capacity of lithium primary battery cell has been improved to 500 Wh/kg. There are many kinds of primary cells with a number of electrodes being tested, but only a few type of electrodes were selected due to practicality [1]. Table 1.1 shows the characteristics and comparison of different primary batteries.

Table 1.1 Characteristics of major Primary batteries [1]

System	**Zinc-carbon (Leclanche ʾ)**	**Zn / Alk. /MnO2**	**Zn /HgO**	**Zinc / air**	**Li /MnO2**
Anode	Zn	Zn	Zn	Zn	Li
Cathode	MnO2	MnO2	HgO	O2 (air)	MnO2
Electrolyte	NH4Cl and ZnCl2 (aq)	KOH (aq)	KOH or NaOH (aq)	KOH (aq)	Organic solvent, salt solution
Cell voltage (V)	1.5	1.5	1.35	-	3
Specific Energy (Wh/ kg)	85	145	100	-	230
Energy Density (Wh/L)	165	400	470	-	533

1.3.2 Secondary Batteries

Secondary batteries are also known as rechargeable batteries. The electrochemical reaction in the cells is reversible and able to convert chemical energy into electrical

energy and vice versa. There are several criteria when designing and manufacturing a rechargeable battery, such as good cycle life, high specific energy, low resistance in external or internal, and good operating temperature [1]. Table 1.2 shows the comparison of rechargeable batteries.

Table 1.2 Characteristics of major rechargeable batteries [1]

System	**Lithium Ion**	**Nickel Metal-Hydride**	**Lead Acid**	**Nickel-Cadmium**	**Zinc / air**
Anode	Carbon (Graphite)	Metal-Hydride	Lead Alloy	Cadmium	Zn
Cathode	$LiCoO_2$	Nickel oxyhydroxide	Lead dioxide	Nickel oxyhydroxide	O2 (air)
Electrolyte	Organic solvent, salt solution	Aqueous KOH, polypropylene	Aqueous H_2SO_4, polyethylene	Aqueous KOH, polypropylene	Aqueous KOH
Nominal voltage (V)	3.6	-	2	-	-
Energy density (Wh/ L)	260	220	70	60-100	200
Power Density (W/L)	400-500	475	~400	220-360	190
Cycle Life	500-1000	300-600	250-500	300-700	~200

One of the most popular secondary batteries is the lead-acid battery. It is also the first type of secondary battery being developed due to its low cost, ease of manufacturing, and good cycle life. The common application of lead-acid battery can be seen in the automotive industry. The issue with it is the low energy density. Besides that, if the battery is inactive for a long period or the operating temperature is too high, the performance will decline greatly. To recover the performance, the electrolyte is being removed by dry-charged and the cell will be activated by filling in the electrolyte [2].

The two types of nickel battery, Nickel-Cadmium (Ni-Cd) and Nickel-metal hybrid (Ni-MH) battery shown in Table 1.2 are categorized as alkaline rechargeable batteries. The common application of Ni-Cd batteries are in the field of diesel engines, emergency power applications, and aircrafts. The advantages of this nickel battery are great cycle life, stable operation voltage, high rate of discharging, and low operating temperature. Conversely, its disadvantages are high cost, high maintenance, and environmentally issue as Cd are not environmentally friendly.

Nickel-metal hydride batteries are somewhat similar to Nickel-Cd batteries. This metal alloy improves the energy density and decreases environmental issues. During charging process, metal hydrides are formed by absorbing hydrogen. Vice versa, hydrogen is produced in the opposite process. Therefore, this system is a reversible process. Because of its good cycle life and low depth of change, it is often used in aerospace applications. However, the drawbacks are high cost and low tolerance for overcharges compared with Ni-Cd battery [3].

The first commercialized rechargeable Li-ion batteries are produced by Sony Company in 1991. The active materials used are LiCoO2 as cathode and graphite as anode. These Li-ion batteries have high energy density and are often used in portable electronic devices. Later on, Li-ion battery move forward to large scale applications such as hybrid electric vehicles (HEV). More details of Li-ion battery presented in these reference papers [1, 4].

1.4. Rechargeable Li-ion Batteries

1.4.1 Operation Principles

The current Li-ion batteries on the market do not have lithium metal in them. Instead, the anode side is made of a carbon-based material. The cathode side contains a lithium transition metal oxide. Liquid electrolyte is used as an ionic conductor to provide movement of lithium ions to pass through the cell. Figure 1.3 illustrates a schematic of a Li-ion battery during the charge and discharge processes.

Graphite acts as a host for lithium ions that are crossing over to the cathode side through the electrolyte during the charging process, while electrons travel to the anode side by passing through an external circuit. Conversely, cathode material will be the host to accept the lithium ions from the anode during the discharging process [5, 6].

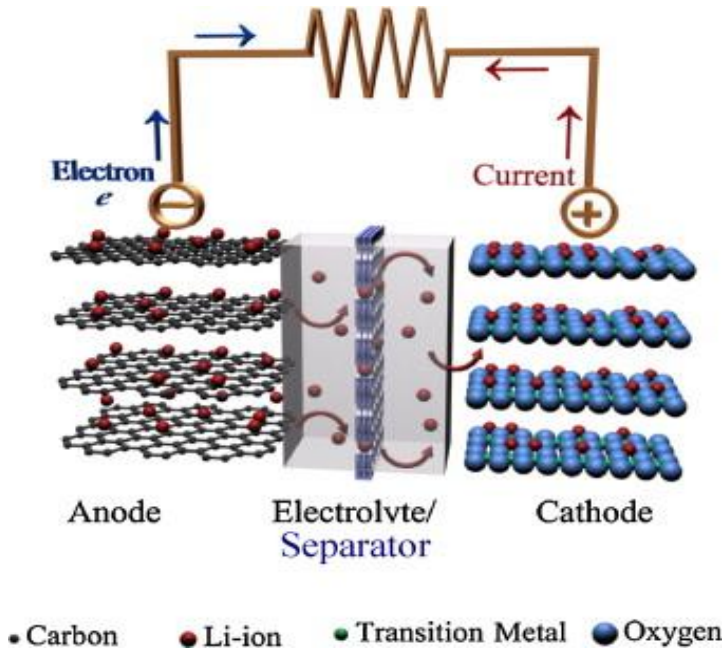

Figure 1.3 Schematic of a Li-ion battery during operation [1]

For the development of rechargeable Li-ion batteries, materials selection for both anode and cathode are very important and it is a major challenge to researchers. Figure 1.4 illustrates an open circuit energy diagram for a thermodynamically stable non-aqueous electrolyte cells. The band gap of electrolyte E_g is the energy difference between the unoccupied molecular orbital (LUMO) and the highest occupied molecular orbital (HOMO). μ_A and μ_C are the electrochemical potentials for both anode and cathode. Both μ_A and μ_C are required to fall between LUMO and HOMO of the electrolyte. In the case of anode with μ_A higher than LUMO level and a cathode with μ_C lower than HOMO level, the electrolyte will decompose. To prevent that, a stable passivation solid electrolyte interface (SEI) layer is needed to prevent electron transfer from the anode to the LUMO or from the HOMO to the cathode. The open circuit voltage V_{oc} of a battery cell can be distinguished by calculating the difference between the electrode electrochemical potentials:

$$V_{oc} = \frac{\mu_C - \mu_A}{e}$$

e = the amount of electron charge [5].

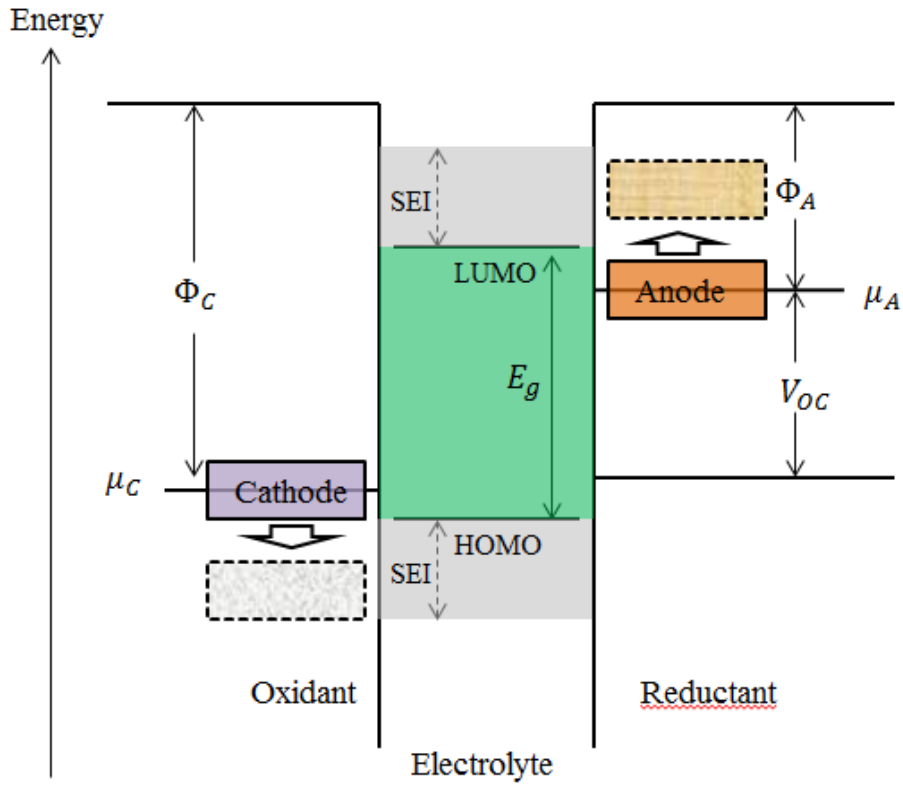

Figure 1.4 Electrochemical window for thermodynamically stable aqueous electrolyte cells [5]

The specific capacity Λ of a Li-ion battery is defined as reversible charge transfer per unit weight (Ah/g) between the electrodes. Energy density is then defined as ΛV.

Liquid provides high mobility for ion movement. The electrochemical window of H_2O is approximately 1.23eV which limits the open circuit voltage of the cell. A non-aqueous electrolyte with a large electrochemical window is required in order to obtain higher energy density. To do this, the LUMO and HOMO level of the non-aqueous electrolyte should be well researched so that the electrode potential falls within the gap. Although lithium metal is a great anode material, its electrochemical potential is located above the LUMO level. To overcome this problem, passivation SEI layer is used to allow

usage of lithium metal as an anode in the cell. One of the major problems with using lithium metal is the dendrites issue. Dendrites will be formed when lithium metal undergoes a charge and discharge process for a certain period of time and the cell could be shorted. In order to prevent that from happening, the potential of anode and cathode must be kept within the electrochemical window of electrolyte and ensured the SEI layer must have fast ionic conduction capability [5].

The goals of development of rechargeable Li-ion batteries are to achieve low cost, better safety, and high energy and power densities.

1.4.2 Components of the Lithium-ion Battery Cell

1.4.2.1 Electrolytes

Electrolytes serve as a medium for the transport of ions. Material selection for electrolyte will greatly affect the performance of the battery. The volume of electrode will keep expand and contract during charging and discharging process, therefore a good electrolyte with good stability for electrode and electrolyte interface is needed. The ionic conductivity of the lithium ion needs to be higher than 10^{-4} S/cm and electronic conductivity is desired to be smaller than 10^{-10} S/cm. The ideal electrolyte should not react with anode and cathode materials should be cheap in cost, non-toxic, and nonflammable. Researchers face the challenge of finding an electrolyte with a wide electrochemical window and a good stability at practical temperature [1, 5].

Each application requires different types of electrolytes as they have different properties. Table 1.4 illustrates different types of electrolytes with their ionic conductivity and the electrochemical window.

Table 1.3 Non-aqueous Electrolytes for Li-Ion Batteries [5]

Electrolytes	Example of electrolytes	Ionic conductivity ($\times 10^{-3}$ s/cm) at room temp	Electrochemical window (V) vs Li+/Li0		Property	Reference
			Reduction	Oxidation		
Liquid organic	1M $LiPF_6$ in EC:DEC (1:1)	7	1.3	4.5	Flammable	[7-9]
	1M $LiPF_6$ in EC:DMC (1:1)	10	1.3	>5	Flammable	[8, 9]
Ionic liquids	1M LiTFSI in EMI-TFSI	2	1	5.3	Non-flammable	[10]
	1M $LiBF_4$ in EMI-BF_4	8	0.9	5.3	Non-flammable	[4, 10]
Inorganic liquid	$LiAlCl_4 + SO_2$	70	-	4.4	Non-flammable	[2]
Inorganic solid	$Li_{3.25}Ge_{0.25}P_{0.75}S_4$	2.2	<0.0	>5	Non-flammable	[11]
Polymer	LiTFSI-P(EO/MEEGE)	0.1	<0.0	4.7	Flammable	[12]
	$LiClO_4$-PEO_8 + 10 wt % TiO_2	0.02	<0.0	5	Flammable	[13]
Liquid organic + Polymer	$LiClO_4$ + EC + PC + PVdF	3		5	-	[14]
Ionic liquid + Polymer	1M LiTFSI + P_{13}TFSI + PVdF-HFP	0.18	<0.0	5.8	Less Flammable	[15]
Ionic liquid + Polymer + Liquid organic	56 wt % LiTFSI-Py_{24}TFSI + 30 wt % PVdF-HFP + 14 wt % EC/PC	0.81	1.5	4.2	Less Flammable	[16]
Polymer + Inorganic solid	2 vol % $LiClO_4$-TEC-19 + 98 vol% 95 ($0.6Li_2S + 0.4Li_2S$) + $5Li_4SiO_4$	0.03	<0.0	>4.5	Non-flammable	[17]
Ionic liquid + Liquid organic		-	-	-	Non-flammable	[3]

1.4.2.1.1 Liquid Electrolyte

Liquid electrolytes specifically organic liquid electrolyte are a solution of an ion-forming inorganic lithium compound in a mixture of a high-permittivity solvent and a low-viscosity solvent. Organic liquid electrolytes contain carbonate liquids in which lithium salts are soluble[8, 18], with an HOMO level at 4.7V [7, 19] and an LUMO level at 1.0V [9]. Besides that, due to low viscosity, it has small activation energy of ion diffusion. Liquid electrolytes can be made from mixing two or fewer carbonates such as ethylene carbonate (EC), diethyl carbonate (DEC), ethylmethyl carbonate (EMC), propylene carbonate (PC), or dimethyl carbonate (DMC). One of the properties of Ethylene carbonate is that a stable SEI layer will form on graphite anode to prevent electrolyte decomposition [20, 21].

1.4.2.1.2 Solid Electrolytes

Solid electrolytes are studied due to their safety reasons. These solid electrolytes have a large range of electrochemical windows. The most common types of solid electrolytes are solid polymers and ceramics. Ceramic electrolytes are applied for thin film devices due to their high elastic moduli and rigid design. In addition, high conductivity at high temperature and stability in extreme environments are also the properties of ceramic electrolytes. In room temperature conditions, ceramics provide low ionic conductivity, resulting in low cell rate capability. For solid polymer, it has lower elastic moduli compared to ceramics. It is light, has low manufacturing costs, and is easy to fabricate. Similar to ceramics, polymer electrolytes have low ionic conductivity at room temperature. Extensive research has been done in terms of increasing the conductivity at room temperature [22].

There are 3 categories of ceramic electrolytes which are sulfides, phosphates, and oxide ceramics. The ionic conductivity of ceramic electrolytes can be increased by raising the temperatures. This is due to the energy generated from heat that causes the

ions inside the ceramics to move around. Hence, they are suitable for application at high operating temperatures.

One example of sulfide ceramic electrolytes is glass ceramic such as Li_2S-P_2S_5. The crystalline phase of Li_2S-P_2S_5 has lower activation energy and better ionic conductivity [23-25]. The $Li_{3.25}Ge_{0.25}P_{0.75}S_4$ lies in the thio-LISICON group and is another type of sulfide crystal reported in the papers [26, 27]. The perovskite (La,Li)TiO3 or LLTO is a good lithium ion conductor [28-30]. The electrochemical window and lithium ion conductivity of oxide ceramics can be increase by doping LLTOs [31-33].

The phosphate ceramics are the better than sulfide and oxide ceramics. This is because of their high conductivity. One example of a phosphate ceramics electrolyte is NASICON. The $Li_{1+x}Al_xGe_{2-x}(PO_4)_3$ (LAGP) were reported to have the highest conductivities [34-36].

1.4.2.2 Separator

The function of a separator is to prevent electrodes from directly contacting each other inside the cell which will lead to short circuit. The two commercial separators are Polypropylene (PP) and Polyethylene (PE). They are microporous membrane separators. The separators have a function to prevent Li-ion batteries from overheating. The separator has a shutdown mechanism that prevents the thermal behavior of a battery when the battery is overcharged, causing large heat generation. This can be done by switching porous polyolefin to non-porous insulator between electrodes when the temperature of the separator reaches a shutdown point. PE separators shutdown point is about 130 ℃ to 140 ℃. However, both PE and PP have their shutdown temperatures close to meltdown temperature. The separator will lose its mechanical properties once it reaches the meltdown temperature. PP meltdown temperature is around 170 ℃ [37, 38]. Intensive studies have been carried on to improve the performance of separators by increasing the meltdown temperature [39].

1.4.2.3 Electrodes

For a good battery design, electrodes have to be chemically stable with electrolytes. To do so, the electrochemical potential of the electrodes have to fall within the LUMO and HOMO level of electrolytes. Electrodes have the capability to host lithium ions. The first reported Li-ion battery contained $LiCoO_2$ and petroleum cole electrodes [12]. Figure 1.5 shows voltage and specific capacity of electrodes, as well as an electrochemical window of 1M $LiPF_6$ in EC/DEC organic liquid electrolytes [5].

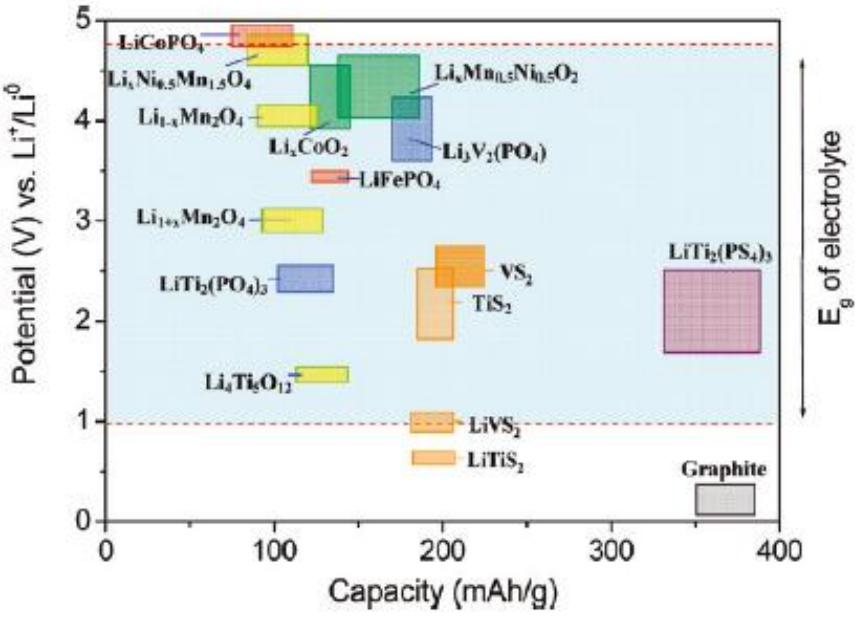

Figure 1.5 Voltage versus capacity of common electrode materials relative to electrochemical window of 1 M $LiPF_6$ in EC/DMC [5]

1.4.2.3.1 Anode

Selecting the right materials for anode is essential to obtain high energy density cells. Lithium based anodes are currently the best option for Li-ion batteries. Among other metals, lithium has the lightest weight and this serves as a good material for anodes. Lithium has high specific capacity of 3862 mAh/g due to its low density. The application of lithium metal in battery system can be seen in many portable devices. Unfortunately, the usages of lithium anodes have some challenge due to safety reasons. During the

charging process, dendrites will form and that will cause short circuit by penetrating the separator [11, 13, 14].

In the searching for alternative anode materials, carbonaceous materials would be the next option. They have low electrochemical potential, high capacity, and high electronic conductivity. Graphite allows for good intercalation of lithium with the properties of layered structure. In addition, graphite is not expensive and provides high specific capacity of 372 mAh/g. All these properties make graphite a suitable alternative anode material for Li-ion batteries [40].

Recently, silicon becomes an alternative material to substitute graphite anodes. Silicon has high theoretical capacity of 4200 mAh/g with operation voltage of 0.4 V, but the high expansion and contraction (more than 300%) during charging and discharging causes big problems. The expansion and contraction cause electrodes to crack and lose contact with electronic current collector. This causes a great decrease in cycle life. Researchers try to use Si nanowires to increase the cycle life but the capacity still drops significantly after some cycles [41].

$Li_4Ti_5O_{12}$ is another alternative material for anode with the theoretical specific capacity of 175 mAh/g and with 1.5 V of operation voltage. $Li_4Ti_5O_{12}$ has the feature of zero-strain material due to its low variation of lattice parameter during lithium intercalation [42]. This provides a good long cycle life. Table 1.3 shows properties comparison of a few anode materials.

Table 1.4 comparison of selected anode materials [43]

Materials	**Li**	**C**	**$Li_4Ti_5O_{12}$**	**Si**
Density (g/cm^3)	0.53	2.25	3.5	2.33
Lithiated phase	Li	LiC_6	$Li_7Ti_5O_{12}$	$Li_{4.4}Si$
Theoretical specific capacity (mAh/g)	3862	372	175	4200
Theoretical charge density (mAh/cm^3)	2047	837	613	9786
Volume change (%)	100	12	1	320
Potential vs. Li (~V)	0	0.05	1.6	0.4

1.4.2.3.2 Cathode

Among the commercial Li-ion batteries, the most common electrode is $LiCoO_2$. It has a flat operation voltage of 3.9 V compared with lithium and about 140 mAh/g specific capacity. This is half of the theoretical capacity, meaning that only half of the lithium ion can go back and forth. Figure 1.6 shows the layered structure with fast two dimension diffusion of lithium ions. A lot of research was done on the development of materials with high rechargeable capacities and high energy density which can be compatible with $LiCoO_2$ [44]. Other than that, $LiCo_{1/3}Ni_{1/3}Mn_{1/3}O_4$ is also a potential cathode material with a capacity of 200 mAh/g. The voltage of $LiCo_{1/3}Ni_{1/3}Mn_{1/3}O_4$ is reported to be lower than $LiCoO_2$, but the energy density is equal or more than $LiCoO_2$ [45].

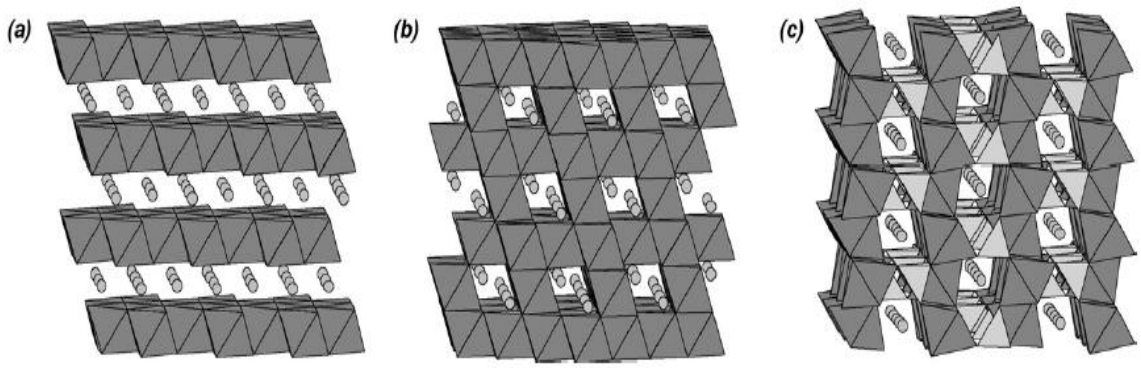

Figure 1.6 Crystal structures of (a) Layered structure ($LiCoO_2$), (b) Spinal structure ($LiMn_2O_4$), and (c) Olivine structure ($LiFePO_4$) [46]

Intensive research has been done on $LiMn_2O_4$ (Figure 1.6 (b)). It has high flat operation voltage of 4.1 V and the theoretical capacity of 148 mAh/g which is higher than $LiCoO_2$. There are other Manganese-base spinal structure materials being studied as well. For example, the $LiNi_{0.5}Mn_{1.5}O_4$ with very flat operation voltage of 4.7V and practical capacity of 135 mAh/g can be an alternative for advanced Li-ion battery systems [47].

$LiFePO_4$ is also a potential cathode material for Li-ion batteries. Figure 1.6 (c) shows the olivine structure of $LiFePO_4$. It became a popular material due to its low cost and less toxic amount of Fe when compared with other cathode materials. The rechargeable capacity of $LiFePO_4$ is reported to be 160 mAh/g with extremely flat operation voltage about 3.5 V. In addition, it is chemically stable and has a long cycle life to about 1000 cycles without significant change in capacity. Despite its low energy density, $LiFePO_4$ has low sensitivity when temperature changes and it is also proven to have better safety compared with $LiCoO_2$. The drawbacks of $LiFePO_4$ are its low ionic and electronic conductivity at room temperature. Studies have been carried on to improve the conductivities by decreasing the particle size and applying carbon coating. Nanosize $LiFePO_4$ particles coated with conductive carbon provides a capacity close to the theoretical one and it has better cycling performance [48-50]. Figure 1.7 shows charge

and discharge curves of several cathode materials tested in non-aqueous liquid electrolytes [46].

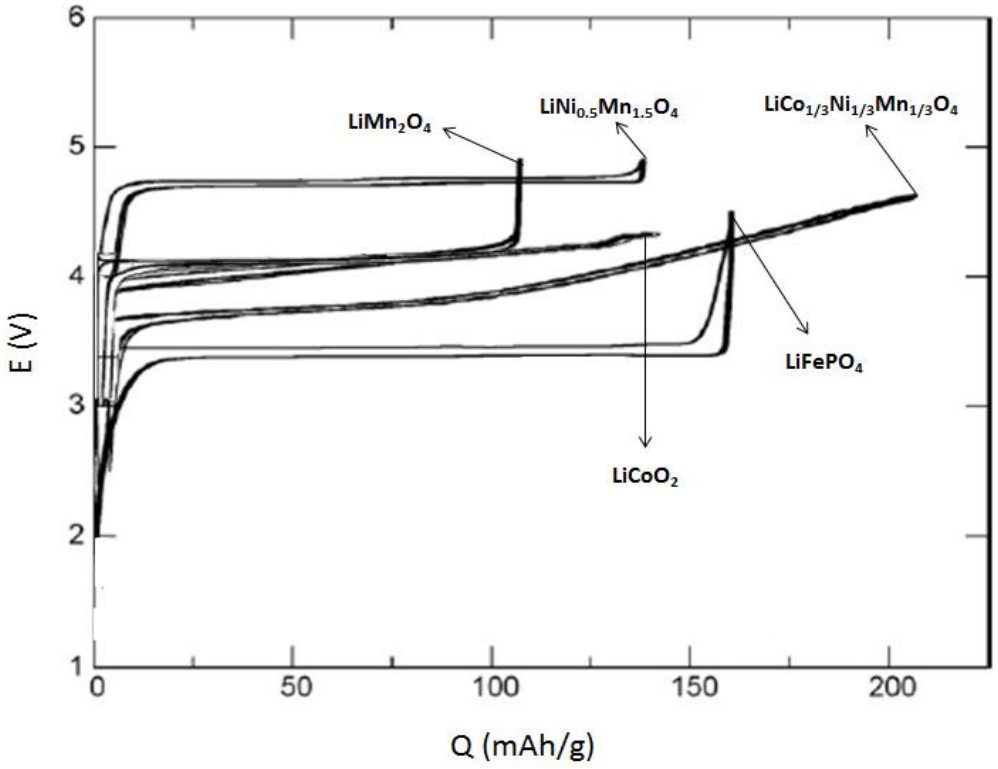

Figure 1.7 Charge and discharge graphs of $LiCoO_2$, $LiMn_2O_4$, $LiCo_{1/3}Ni_{1/3}Mn_{1/3}O_4$, $LiNi_{0.5}Mn_{1.5}O_4$, and $LiFePO_4$cathode materials tested in non-aqueous liquid electrolyte [46]

CHAPTER 2. CHEMICAL TRANSFORMATION FROM $NAVS_2$ TO β-$NA_{0.33}V_2O_5$ AND ITS FULLY REVERSIBLE LI-INTERCALATION

2.1 Introduction

Vanadium pentoxide, V_2O_5, was one of the first oxides to be studied for use as a cathode in lithium (Li) ion batteries because its structure consists of VO_5 square pyramids layers with an open Li intercalation site between the layers. In addition, its open structure could combine with the wide range of oxidation states for vanadium, ranging from V5+ to V3+, which allows for a high theoretical specific capacity of 442 mAh/g for $Li_xV_2O_5$ when x = 3 [51-53] . However, vanadium pentoxide's practical reversible capacity has been limited due to its irreversible structural change when Li insertion is more than x =1[54]. Great effort has been made over the last twenty years to improve the phase reversibility of $Li_xV_2O_5$ (e.g. $0 \leq x \leq 2$) by influencing the compound's structure and surface defects as well as its particle size and morphology. Such influence has been created by applying many different methods of synthesis and post-treatment conditions, respectively [55-58].

One of the trials found that a better stable and rigid 3D framework structure with a tunnel was achieved by doping with metallic species (such as Na) into the V_2O_5, producing β-$Na_{0.33}V_2O_5$ [59, 60]. The β-$Na_{0.33}V_2O_5$ contains three different open intercalation sites in its 3D tunnel structure where Li can be reversibly intercalated at the range of $0.0 \leq x \leq 1.66$. And, all of the phase transformations observed in the Li_xβ-$Na_{0.33}V_2O_5$ are reversible during cycling when $0.0 \leq x \leq 1.66$, which provide the specific capacity up to 234 mAh/g at x = 1.66. Many types of synthesis methods for the β-$Na_{0.33}V_2O_5$, which include solid-state reaction [61, 62], sol-gel method [63-65], and hydrothermal method [60, 66, 67], has been attempted to advance its electrochemical performances. However, to the best of our knowledge, the Na extraction from the

$Na_{0.33}V_2O_5$ has not reported elsewhere. If possible without structure collapse, more than 1.66 Li can be intercalated into the structure of the $Na_{0.33}V_2O_5$, which can improve the specific capacity more than 234 mAh/g.

In this work, the β-$Na_{0.33}V_2O_5$ was synthesized via a new chemical route involving a chemical transformation of the $NaVS_2$ heat-treated at 600 ℃ in atmospheric air for the first time. The prepared samples were well crystalized and rod-shaped, measuring 7–15 μm long and 1–3 μm wide. Surprisingly, the Na ions of the β-$Na_{0.33}V_2O_5$ were fully extracted from the compound's structure. And, without the phase irreversibility, subsequent intercalation of Li ions into $Li_xV_2O_5$ was observed when $0.0 \leq x \leq 2.0$. This delivered 300 mAh/g capacity at a 0.1 mA/cm^2 between 1.5 V and 4 V and 91% capacity retention after 50 cycles. When considering the particle sizes of the β-$Na_{0.33}V_2O_5$ phase, its observed electrochemical performance is surprising. The phase evolution of β-$Na_{0.33}V_2O_5$ caused by heat-treating the pure sulfide, and the resultant enhanced electrochemical performances will be discussed further.

2.2 Experimental Methods

2.2.1 Preparation of the Samples

To prepare the $NaVS_2$, appropriate amounts of Na_2S (Sigma, 99%), vanadium (Alfa, 99.5%), and sulfur (Sigma, 99.99%), respectively, were mixed altogether and placed in a carbon-coated quartz tube inside an Ar glove box. Then, the quartz tube was sealed under vacuum. The sealed tube was slowly heated over 20 h to 700 ℃ , next kept for 40 h at 700 ℃, and then slowly cooled over 5 h to 250 ℃, followed by quenching the tube in air. While inside an Ar glove box, the samples were removed from the tubes and then thoroughly ground and pelletized. Next, the samples themselves were treated to the same experimental process (and at the same temperatures) as the tubes were treated to. Because the $NaVS_2$ is sensitive to moisture, it was always handled in an Ar atmosphere.

To prepare the vanadium oxides, the $NaVS_2$ powders that were loaded in an Al_2O_3 crucible were moved out of the glove box and then placed into the furnace in atmospheric air. The powders were slowly heated over 5 h to reach 400 ℃ and 600 ℃, respectively, and held for 10 h at each of these temperatures, followed by allowing them to naturally cool to room temperature.

2.2.2 Structural Analysis of the Samples

The powder x-ray diffraction (XRD) data was collected using the Bruker D8 Advanced diffractometer equipped with Cu-Kα radiation and a diffractometer monochromator that was operated at 40 kV and 40 mA. The samples were finely ground and placed in the sample holder of the diffractometer. The morphology of the sample particles were analyzed by scanning electron microscopy (SEM), and the particle surfaces were further characterized using transmission electron microscopy (TEM). The TEM microscope was an aberration-corrected JEOL JEM-2100F operated at 200 kV. Samples were made suitable for TEM observation by grinding the heat-treated material into fine powders and dusting them onto lacy-carbon coated copper TEM grids.

2.2.3 Electrochemical Analysis of the Samples

The electrode disks and cell were all prepared in an Ar glove box. The electrodes were fabricated from a 70:20:10 (wt%) mixture of active material, acetylene black as current conductor, and poly (tetrafluroethylene) as binder. First, the active material and conductor were completely mixed. Then, the binder was added, and the mass was mixed again. The mixture was rolled into thin sheets and punched into 7 mm diameter circular disks to be used as electrodes. The typical electrode mass and thickness were 7-12 mg and 0.03-0.08 mm, respectively. The electrochemical cells were prepared with standard 2016 coin cell hardware, using Li metal foil as both the counter and reference electrodes. The electrolytes used for analysis were 1M $LiPF_6$ in 1:1 EC:DEC. The sealed cells were taken out of the Ar glove box and placed in a battery testing system. The cells were then

aged for 5 h before the first discharge (or charge) to ensure full absorption of the electrolyte into the electrode. A 10 min rest period was taken between the charge and discharge steps.

2.3 Results and Discussion

2.3.1 Chemical and Structural Characterizations of the Samples

This study takes a unique approach to synthesizing a high quality sodium vanadium bronze, β-$Na_{0.33}V_2O_5$, with enhanced crystallinity, via the chemical transformation of $NaVS_2$ heat-treated in air. The pristine $NaVS_2$ sample has the hexagonal structure, consisting of hexagonal-close-packed sulfur with V and Na atoms in alternate octahedral-site (001) planes forming a layered structure [68, 69]. The XRD patterns of the $NaVS_2$ sample (Figure 2.1) matched well to those reported in the literature, and such details of their crystal structures were discussed [68, 69].

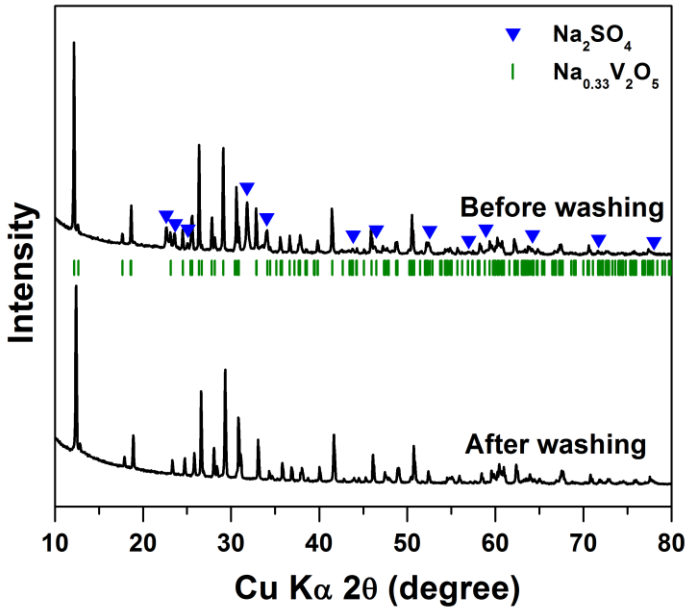

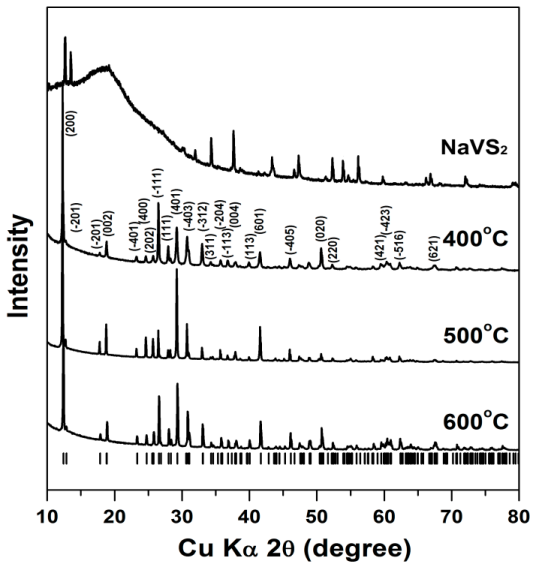

Figure 2.1. (a) Powder XRD patterns of samples heat-treated at 600°C, before and after washing, respectively. (b) Powder XRD patterns for NaVS2 and its samples that were heat-treated for 10 h in air at different temperatures.

When the $NaVS_2$ sample was exposed to atmospheric air and heated at high temperature at 600 ℃ for 10 h, the initial sulfide phase became the mixtures of Na_2SO_4 and β-$Na_{0.33}V_2O_5$ as identified by the XRD in Figure 2.1. The minor phase of the Na_2SO_4 was produced as a result of $NaVS_2$ decomposing during heat-treatment in air, and the Na_2SO_4, was eliminated by washing with water as shown in Figure 2.1. The sample prepared at 400 ℃, 500 ℃, and 600 ℃ was washed with water to remove the Na_2SO_4 phase. Figure 2.1 shows XRD patterns of the washed samples. The XRD data from all three samples (400 ℃, 500 ℃, and 600 ℃) can be indexed based on the β-$Na_{0.33}V_2O_5$ phase with a monoclinic symmetry (space group: C2/m), which has a three-dimensional tunneling structure along the [010] direction. Table 2.1 lists the structural information obtained from a least-square fitting of the XRD data. These results indicate that the chemical and phase transformations of $NaVS_2$ into β-$Na_{0.33}V_2O_5$ appeared by air oxidation of the $NaVS_2$ at temperatures in the range of 400 ℃ - 600 ℃.

Table 2.1. Structural parameters of powder samples obtained after heating for 10 h at 400 ^{o}C – 600 ^{o}C.

Heating Temp.	Phase	Space group	a (Å)	b (Å)	c (Å)	β (degree)	Unit cell volume (Å^3)
400^{o}C	β-$Na_{0.33}V_2O_5$	*C*2/*m*	15.381	3.609	10.072	109.552	526.80
500^{o}C	β-$Na_{0.33}V_2O_5$	*C*2/*m*	15.343	3.608	10.068	109.378	525.77
600^{o}C	β-$Na_{0.33}V_2O_5$	*C*2/*m*	15.362	3.612	10.073	109.383	527.28

Figure 2.2 (a) shows a SEM image, consisting of submicron-sized, rod-shaped particles, of the 400 ℃ sample after washing. On the other hand, the 600 ℃ sample (see Fig. 2.2 (b)) was well crystalized and rod-shaped with a length of 7–15 μm and a width of 1–3 μm. A higher magnification SEM image in Fig. 2.2 (c) shows that the 600 ℃ sample particles have surface defects in the shape of crystals around the edges of the particles, which exposes layers of grains (highlighted with a yellow dotted line). The high-resolution TEM image in Fig. 2.2 (d) also shows the layered grains along the crystal defects. Another TEM image in Figure 2.3 reveals that the longitudinal surface of the rod-shaped particle is (001) where a considerable amount of stacking faults are parallel to the face. It is plausible that the surface area having crystal defects could be interfaced with Na_2SO_4 salt during heat-treatment at 600 ℃, in which the rod-shaped β-$Na_{0.33}V_2O_5$ crystals appeared. The surface defects could be exposed after removing Na_2SO_4 by washing the sample in water.

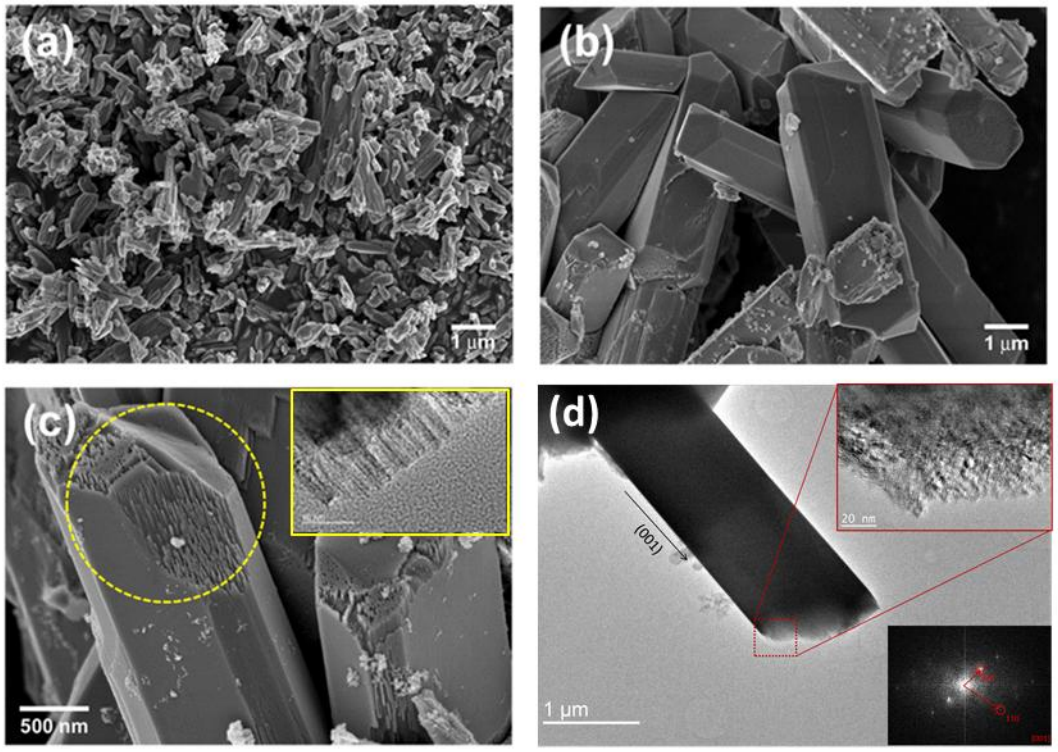

Figure 2.2. SEM images of (a) the 400 ^{o}C sample after washing and (b)-(c) the 600 ^{o}C sample after washing. The crystal defects were observed on the surface of the rod-shaped crystals, as circled in yellow in (c), where high-resolution TEM image was taken. (d) TEM image of a rod-shaped particle of the β-$Na_{0.33}V_2O_5$, which reveals that the longitudinal surface of the particle is (001), and a considerable amount of stacking faults exist parallel to this face.

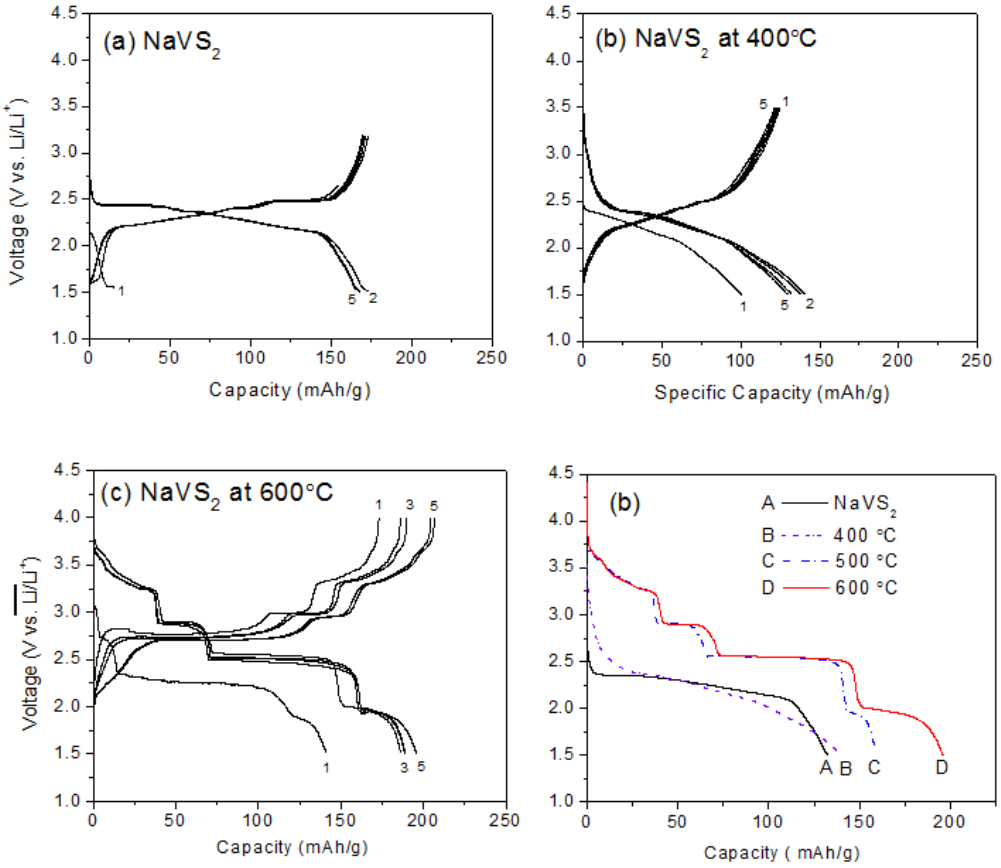

Figure 2.3. Result of (a) Charge-discharge voltage curves of the $NaVS_2$. Charge-discharge voltage curves of the heat-treated $NaVS_2$ at (b) 400 ℃ and (c) 600 ℃. (d) Comparison of second discharge voltage curves of the untreated $NaVS_2$ and the heat-treated $NaVS_2$ at 400 ℃, 500 ℃, and 600 ℃. They were measured at 0.1 mA/cm2.

2.3.2 Electrochemical Characterizations of the Samples

The electrochemical intercalation of Li into the $NaVS_2$ structure was first studied by using the coin cell consisting of Li/1M $LiPF_6$ in EC:DEC/$NaVS_2$. When the cell was discharged first by Li insertion into the $NaVS_2$ structure, a small capacity of ~10 mAh/g was observed, as shown in Fig. 2.4 (a). This indicates that our as-prepared $NaVS_2$ product is Na-deficient, which is commonly observed in lithium- or sodium-layered sulfide compounds prepared via a high temperature solid-state reaction [69, 70]. When the cell was charged after the first discharging, a specific capacity of ~175 mAh/g was observed

by oxidizing V3+ to V4+ via the extraction of cations. The following discharge and charge processes are reversible during cycling of the cell in the voltage range of 1.5 V to 3.2 V at the current rate of 0.1 mA/cm^2. The observed voltage steps are identical to those reported in a previous study of Li_xVS_2 [69, 70].

When the $NaVS_2$ was heat-treated in atmospheric air, the voltage curves of the heat-treated samples varied from that of the untreated $NaVS_2$ sample, as seen in Fig. 2.4 (b). The voltage curve of the 600 ℃ sample (Fig. 2.4 (c)), in particular, was quite different from that of the mother sulfide sample. After washing out the impurity phase of the Na_2SO_4 from the 600 ℃ sample, the specific capacity of the 600 ℃ sample was observed to be increased due to the elimination of the electrochemically inactive phase (Na_2SO_4), while maintaining the same voltage steps as shown in Fig. 2.4 (d). The voltage steps observed in Fig. 2.4 (d) corresponds to the phase transformations with Li intercalation into the $Li_x\beta$-$Na_{0.33}V_2O_5$ phase. All of the phase transformations are reversible during cycling, between 1.5 V and 4.0 V.

The four distinct voltage steps were observed at ~ 3.3 V, ~2.9 V, ~2.5 V, and ~2.1 V during the Li insertion into the $Li_x\beta$-$Na_{0.33}V_2O_5$ phase. The first three voltage profiles located at 3.3 V, 2.9 V, and 2.5 V were assigned to the Li ion occupancy of the β-$Na_{0.33}V_2O_5$ structure's particular empty sites, M3, M2, and M1, respectively [65]. The Na ions were initially located at the M1 sites of the β-$Na_{0.33}V_2O_5$ structure. During the discharging of the cell, when the voltage was 3.3 V, the Li ions began to occupy the M3 sites of the $Li_x\beta$-$Na_{0.33}V_2O_5$ structure when $0 < x \leq 0.33$. The second voltage step at 2.9 V was assigned to the half-occupancy by the Li ions of the M2 sites when $0.33 < x \leq 0.66$. And finally, the large voltage plate at 2.5 V was assigned to the filling of the remaining M1, M2, and M3 sites by the Li ions when $0.66 < x \leq 1.67$. Such Li ion distribution to the M sites was reported to be thermodynamically and kinetically more favorable by minimizing the ion-ion repulsive coulombic interactions during Li insertion into the $Li_x\beta$-$Na_{0.33}V_2O_5$ structure [65]. During Li insertion into the β-$Na_{0.33}V_2O_5$, the Na ions of its structure were reported to be very stable so that Na ions couldn't be extracted from its

structure even at higher temperature range (100 - 450 ℃) [63, 71]. As a result, the degree of Li insertion into the Li_xβ-$Na_{0.33}V_2O_5$ structure is 1.67, but the total number of ions in the structure is 2 (0.33Na + 1.67Li).

However, our as-prepared β-$Na_{0.33}V_2O_5$ showed in Fig. 2.4(d) that the specific capacity of 256 mAh/g (after 1st discharging to 1.5 V) was increased to 286 mAh/g (after 5th discharge) that corresponds to x = ~2.0 in Li_xβ-$Na_{0.33}V_2O_5$. The capacity and voltage steps observed in the discharge process are very reversible during the charge process. Since the maximum number of Li ions that can be inserted into the β-$Na_{0.33}V_2O_5$ is x = 1.67, it could be expected that the extra number of x = 0.33 correlates to the Li ions replacing the Na ions located at the M1 sites. This was also observed in the recent electrochemical study of the β-$Na_{0.33}V_2O_5$ nanorods [67], where more than 1.6 Li intercalation into its nanorod structure was observed while extracting Na from the structure when the cell was discharged to 1.5 V. However, in this study [67], the discharge voltage steps observed during Li insertion into the β-$Na_{0.33}V_2O_5$ nanorod were not repeatable during the charge process, which indicated the irreversible phase transformation during the first discharge process.

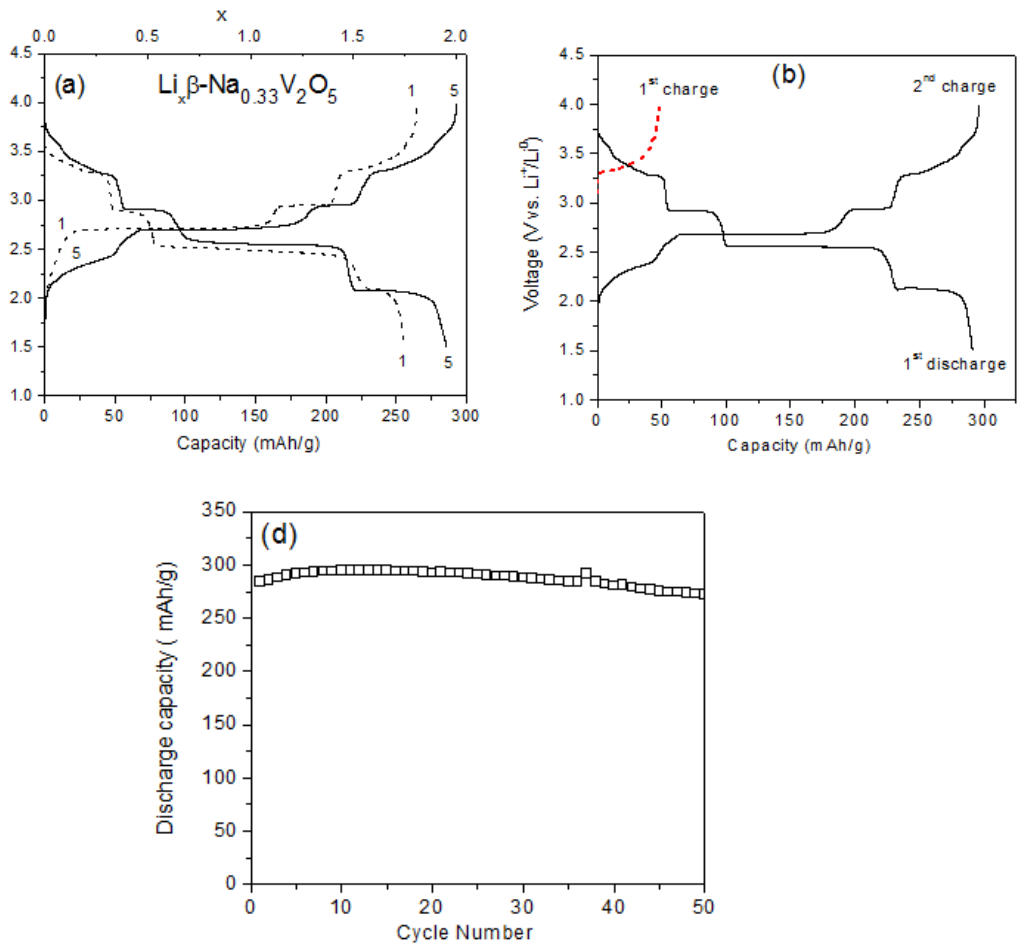

Figure 2.4. Result of (a) Charge-discharge voltage curves of the β-$Na_{0.33}V_2O_5$ at the current rate of 0.1 mA/cm^2. (b) β-$Na_{0.33}V_2O_5$ was charged first to extract Na and followed by Li intercalation into the β-$Li_xV_2O_5$ in the fresh cell by discharging and charging the cell at the current rate of 0.1 mA/cm^2. (c) The cycle-life of the β-$Li_xV_2O_5$ measured at the current rate of 0.1 mA/cm^2.

To confirm the electrochemical extraction of Na from the β-$Na_{0.33}V_2O_5$ structure, the cell was charged first to 4.0 V (see Fig. 2.5 (a)). The charge voltage curve was observed at ~3.3 V, and its capacity (47 mAh/g) corresponds well to the 0.33 Na per unit formula. The following discharge was performed to observe Li insertion into the structure. However, to eliminate the possibility of Na re-insertion into the structure, the Na-extracted electrode was collected after charging the cell and washed in DEC. This

electrode was placed in the fresh coin cell with a Li metal anode and a 1M $LiPF_6$ in EC:DEC electrolyte, which was discharged first to 1.5 V, as shown in Fig. 2.5 (a). In addition to the reported three voltage steps at ~ 3.3 V, ~2.9 V, and ~2.5 V, a fourth voltage step was observed at 2.1 V when the cell was discharged to 1.5 V. In Fig. 2.5 (d), it was shown that the size of the voltage step at 2.1 V is negligible small at the first cycle, but it is getting bigger and eventually saturated after the cell cycled five times. Form these results, it can be expected that the Na ions are extracted from the β-$Na_{0.33}V_2O_5$ during the charge process, and more Li ions are inserted into its structure during discharge process, which results in the capacity increase after five cycles. Hence, the voltage step at 2.1 V can be related to the substitution of Na ions by Li ions in the β-$Na_{0.33}V_2O_5$ structure.

These results were consistent with the EDX measurement collected from the fresh electrode of the β-$Na_{0.33}V_2O_5$ and the electrode charged to 4.0 V. The amount of Na content is the charge β-$Na_{0.33}V_2O_5$ electrode was significantly low compared with that of the fresh electrode as shown in Fig. 2.5 (c).

To the best of our knowledge, this is the first time work that reports the Na ions extraction from the β-$Na_{0.33}V_2O_5$ without irreversible structural change and further reversible Li ions intercalation into its structure in the range of $0 \leq x \leq 2$. Two possible reasons can be expected for the phase reversibility, during cycling, of the β-$Na_{0.33}V_2O_5$ phase. First, the crystal defects formed on the surface of the β-$Na_{0.33}V_2O_5$ phase could stabilize the abrupt structural transformation during Li intercalation when cycling. Similar results were reported when the surface chemistry of the V_2O_5 was modified by coating it with carbon [72] and polypyrrole [73], both showing improved cycle life. Second, the impurities in the crystals, such as the sulfur left inside the structure, could possibly cause the formation of a β-$Na_{0.33}V_2O_5$-ySy. Even a small amount (less than 2 %) of such an impurity could have a significant impact on the Li intercalation properties because impurities stabilize the structure. Examples of impurities include $M_{0.11}V_2O_{5.16}$ with M = Al3+, Fe3+, Cr3+ [74-76]and LiV_3O_8-yX with X = F, Cl [77]. We are planning

a future research project to further characterize the structural and electrochemical behavior of the β-$Na_{0.33}V_2O_5$ phase.

2.4 Conclusion

The highly crystalline β-$Na_{0.33}V_2O_5$ was created via a new method of chemical synthesis, transforming the $NaVS_2$ sulfide by heat-treatment in atmospheric air. Scanning electron microscopy (SEM) revealed that rod-shaped particles were formed during heat-treatment at temperature ranges of 400 ℃ - 600 ℃, and the size of the particles grew at higher temperatures. At the temperature of 600 ℃, rod-shaped particles formed those were 7 – 15 μm long and 1 – 3 μm wide. Moreover, many crystal defects were observed on the surface of the β-$Na_{0.33}V_2O_5$ particles.

The best electrochemical performance was observed in the β-$Na_{0.33}V_2O_5$ prepared at 600 ℃. This sample delivered a high capacity of 285 mAh/g at a 0.1 mA/cm^2 in a voltage range of 1.5 V – 4 V. This electrochemical process corresponds to a reversible insertion/extraction of two Li ($0 \leq x \leq 2$) into Li_xβ-$Na_{0.33}V_2O_5$ by extracting Na from the structure. It should be known that all of the phase transformations with electrochemical Li intercalation in the range of $0 \leq x \leq 2$ were fully reversible. Considering particle sizes of the prepared β-$Na_{0.33}V_2O_5$, the observed electrochemical performances, which include a capacity of 285 mAh/g at a 0.1 mA/cm^2 and 91% capacity retention after 50 cycles, are quite surprising. Although this sample shows a relatively low voltage range compared with other high voltage (> 4.0) cathodes, the large capacity of this sample is quite attractive in terms of increased energy density for Li ion batteries.

Further study is required to understand how the β-$Na_{0.33}V_2O_5$ micro-sized particles prepared in this work provides such a good structural reversibility when $0 \leq x \leq 2$, which have not been reported in any other literature where many preparation methods were attempted.

CHAPTER 3. A NEW CHEMICAL ROUTE FOR THE SYNTHESIS OF β′-LI$_x$V$_2$O$_5$ FOR USE AS HIGH PERFORMANCE CATHODE

3.1 Introduction

Vanadium pentoxide, V_2O_5, is one of the earliest oxides studied as a cathode for Li-ion batteries. Its open structure combined with the wide range of oxidation states for vanadium, which range from V5+ to V2+, allow for a high theoretical specific capacity of 442 mAh/g for $Li_xV_2O_5$ when x = 3 [51-54]. However, its practical reversible capacity has been limited due to its irreversible structural change when Li insertion is more than x = 1 [53, 54]. Tremendous efforts have been made over the last twenty years to improve the phase reversibility of $Li_xV_2O_5$ (e.g., $0 \leq x \leq 2$) because of vanadium pentoxides' potential use as high capacity cathodes in Li-ion batteries [55-58]. Over the course of this research, it was found that the structural and electrochemical behavior of $Li_xV_2O_5$ were very sensitive to the synthesis method and post-treatment conditions that influence its structure and surface defects as well as its particle size and morphology.

For example, when the $Li_xV_2O_5$ was prepared via the high temperature (>400 ℃) solid state synthesis, the phases of α ($0 \leq x \leq 0.04$), β ($0.22 \leq x \leq 0.37$), β′ ($0.44 \leq x \leq 0.49$), and γ ($0.88 \leq x \leq 1$) were subsequently formed by Li insertion into the $Li_xV_2O_5$ [61, 78, 79]. In the same preparation method but at a lower temperature (< 400 ℃), the phases of α ($x \leq 0.1$), ε ($0.35 \leq x \leq 0.7$), δ ($0.9 \leq x \leq 1.0$), γ ($x > 1$), and ω ($x \approx 3.0$) phases were formed [61, 78, 79]. This solid state synthesis method generally produces large V_2O_5 particles with irregular morphology due to particle agglomeration at high temperatures, which generally leads to low capacity and poor cycle life [80]. In order to influence the structural defects of the vanadium oxide and to prevent the irreversible phase transition that occurs when $x > 1$, many other chemical routes have also been made in order to improve the electrochemical performance of V_2O_5. Such methods include electrospinning

[81, 82], polyol [83] and urea combustion [84], and soft-chemical synthesis under milder temperature conditions including a solid-gel process [85], hydrothermal process [86, 87], and hydrolysis [88]. The recently developed urea combustion method yielded 320 mAh/g and 70% capacity retention after 50 cycles at 0.1 C [84]. A recent paper [52]shows that the nano-rod structured V_2O_5 prepared by the hydrothermal process produces 270 mAh/g at 0.5 C and has a 84 % capacity retention after 50 cycles, which is a big improvement when compared with that of the corresponding micro-sized V_2O_5. This continues to be an on-going project in many research groups worldwide because the potential of using V_2O_5 as a high capacity cathode (> 250 mAh/g) in the Li-ion battery is attractive, and it is crucial to develop a high capacity cathode in order to advance present Li-ion batteries.

In this work, a new chemical route for synthesizing vanadium oxides was discovered. The heat treatment of pure $LiVS_2$ in atmospheric air transformed the vanadium sulfide phase to the vanadium oxide phases, β′-$Li_xV_2O_5$ at 600 ℃ and LiV_3O_8 at 700 °C, respectively. The β′-$Li_xV_2O_5$ phase prepared in this method was crystallized into rod-shaped particles with a length of ~20 μm and a width of ~3 μm. The Li intercalation into the β′-$Li_xV_2O_5$ phase is reversible even at deep discharge to 1.5 V and charge to 4.0 V with capacity up to 310 mAh/g (0.07 C). The capacity retention after 50 cycles remains 88% even at 2 C. When considering the particle sizes for the $Li_xV_2O_5$ phase, the observed electrochemical performance is surprising. This phase evolution from the pure sulfide due to the heat treatment conditions and the resulting enhanced electrochemical performance will be discussed further.

3.2 Experimental Methods

3.2.1 Preparation of the Samples

To prepare the $LiVS_2$, appropriate amounts of $Li2_S$ (Sigma, 99%), vanadium (Alfa, 99.5%), and sulfur (Sigma, 99.99%) were mixed and placed in a carbon-coated quartz

tube inside an Ar glove box. Then, the quartz tube was sealed in a vacuum. The sealed tube was heated slowly over 20 h to 700 ℃, kept at 700 ℃ for 40 h, and then cooled slowly over 5 h to 250 ℃, followed by quenching in air. The samples were removed from the tubes, which were inside an Ar glove box where they were thoroughly grounded and pelletized. Then the samples were treated again to the same experimental process at the same temperatures. Because the $LiVS_2$ is moisture-sensitive, it was always handled in an Ar atmosphere.

To prepare the vanadium oxides, the $LiVS_2$ powders that were loaded in an Al_2O_3 crucible were moved out of the glove box and then placed into the furnace in atmospheric air. The powders were heated slowly over 5 h to reach 300 ℃, 500 ℃, 600 ℃, and 700 ℃, respectively, held for 10 h at each of these temperatures, and then cooled naturally to room temperature. Furthermore, the electrochemical performance of the prepared samples was compared with that of the commercial V_2O_5 (99.99%), which was purchased from Aldrich.

3.2.2 Structural Analysis of the Samples

The powder X-ray diffraction data was collected using the Siemens D 500 diffractometer equipped with Cu-K radiation and a diffractometer monochromator that was operated at 45 kV, 30 mA, in step scan mod with a step size of 0.02 °and a step time of 1.5 s. The samples were finely grounded and placed in the sample holder of the diffractometer.

The morphology and the compositional analyses were done by scanning electron microscopy (SEM) and transmission electron microscopy (TEM) equipped with energy dispersive X-ray spectrometry (EDX) and electron energy loss spectrometry (EELS).

The SEM microscope was a JEOL JSM-5310LV operated at 3 kV. The TEM microscope was an aberration-corrected JEOL JEM- 2100F operated at 200 kV. Samples

suitable for TEM observation were made by grounding the heat-prepared material into fine powders and dusting them onto lacy-carbon coated copper TEM grids. JEMS, a Java version of the electron microscopy simulation program, was used to index and calculate diffraction patterns. Time-of-flight secondary ion mass spectroscopy (TOF SIMS) analyses were conducted on a PHI TRIFT V nanoTOF (Physical Electronics, Chanhassen, MN). A 30 kV Au+ primary ion source was used for analyses. All spectra were acquired within the static regime using a total ion dose less than 1011 ions per cm^2. TOF SIMS spectra were collected from areas of 50 μm x 50 μm. At least three sample areas were examined to confirm data reproducibility. During the analyses, the base pressure of the analyses chamber was maintained at less than 2.5×10^{-7} Pa.

3.2.3 Electrochemical Analysis of the Samples

Both the electrode disks and cell were prepared in an Ar glove box. The electrodes were fabricated from a 70:20:10 (wt.%) mixture of active material, acetylene black as current conductor, and poly (tetrafluroethylene) as binder. First, the active material and conductor were mixed completely. Then, the binder was added, and the mass was mixed again. The mixture was rolled into thin sheets and punched into 7 mm diameter circular disks to be used as electrodes.

The typical electrode mass and thickness were 7-12 mg and 0.03-0.08 mm, respectively. The electrochemical cells were prepared with standard 2016 coin cell hardware with Li metal foil used as both the counter and reference electrodes. The electrolytes used for analysis were 1 M $LiPF_6$ in 1:1 EC:DEC. The sealed cells were taken out of the glove box and placed in a battery testing system. They were aged for 5 h before the first discharge (or charge) to ensure full absorption of the electrolyte into the electrode. A 10 min rest period was taken between the charge and discharge steps.

3.3 Results and Discussion

3.3.1 Vanadium Oxide Evolution from the $LiVS_2$

Instead of a conventional solid-state reaction method, this study takes a unique approach to synthesize high quality lithium vanadium bronzes with enhanced crystallinity. Pure $LiVS_2$ has been prepared and heat-treated in air at different temperatures in the range of 300–700 ℃ for 10 h. The crystal structures of the resulting powders were analyzed using XRD and are shown in Fig. 3.1. Because the pristine $LiVS_2$ sample is moisture-sensitive and quickly decays in free air even at room temperature, its powder sample was sealed in a sample holder using a thin amorphous tape in an Ar glove box before measuring the XRD. Resultant XRD patterns of the $LiVS_2$ sample (Fig. 3.1) were indexed as the hexagonal structure, consisting of hexagonal-close-packed sulfur with V and Li atoms in alternate octahedral-site (0 0 1) planes [70]. The XRD pattern closely matches that of published data [JCPDS no. 65-1893].

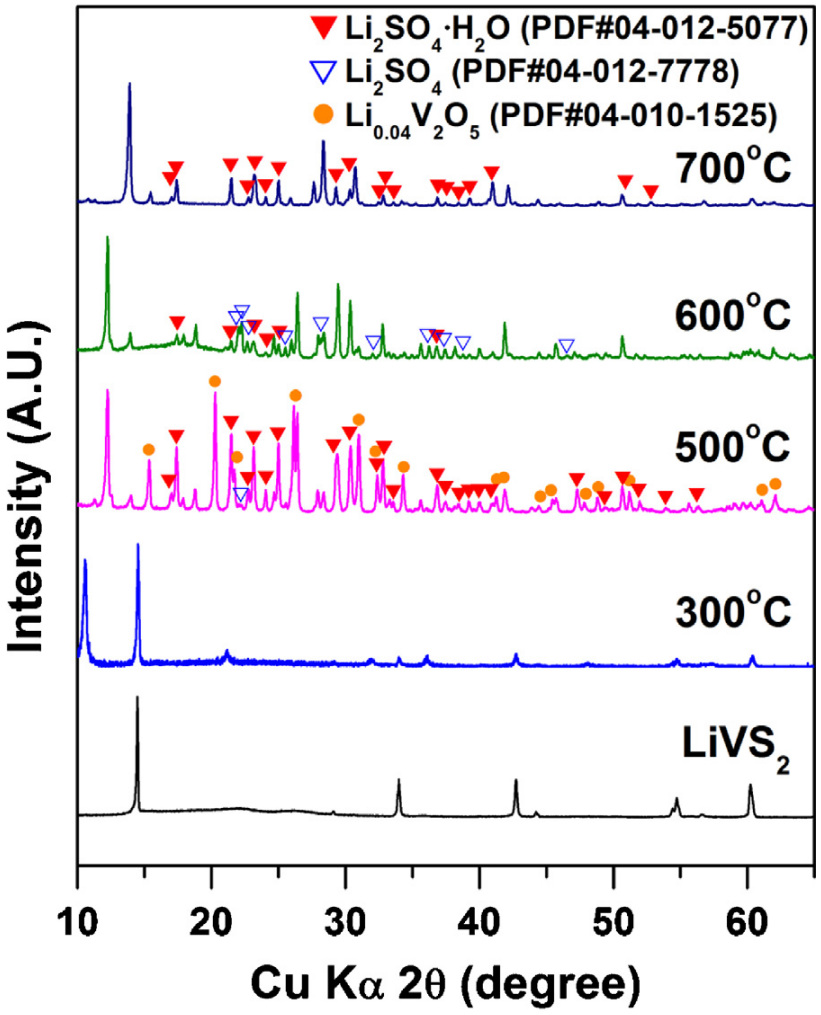

Fig. 3.1 XRD patterns of the pristine $LiVS_2$ and its products that were heat-treated in air for 10 h at 300 ℃ –700 ℃. [89]

When the temperature was increased to 300 ℃, even though the XRD peaks corresponding to the $LiVS_2$ phase still appeared, there was a growth of unknown phases having a strong reflection at $2\Theta \approx 10.5$ °. A further increase in temperature to $T \geq 500$ ℃, however, resulted in a disappearance of both the $LiVS_2$ and the unknown phases. Based on the XRD patterns in Fig. 3.1, the samples that were heat-treated at 500–700 ℃ consisted of mixtures of various lithium vanadate and lithium sulfate phases. The Li_2SO_4 or $Li_2SO_4 \cdot H_2O$ phases were a result of the $LiVS_2$ decomposing in air. However, since the

Li_2SO_4 and $Li_2SO_4 \cdot H_2O$ phases are soluble in water, they were eliminated from the major phases by washing them with water followed by drying them in a vacuum for further structural and electrochemical analysis.

Fig. 3.2 (a) and (b), respectively, compares SEM images before and after washing the samples that were prepared at 600 ℃. Large agglomerates observed in Fig. 3.2 (a) were washed away, and well-grown large crystals were observed in Fig. 3.2 (b). The XRD patterns of the 600 ℃ sample were also compared, before and after washing, as can be seen in Fig. 3.2 (c). The inset of Fig. 3.2 (c) clearly reveals that both the Li_2SO_4 and $Li_2SO_4 \cdot H_2O$ phases vanished after being washed with water.

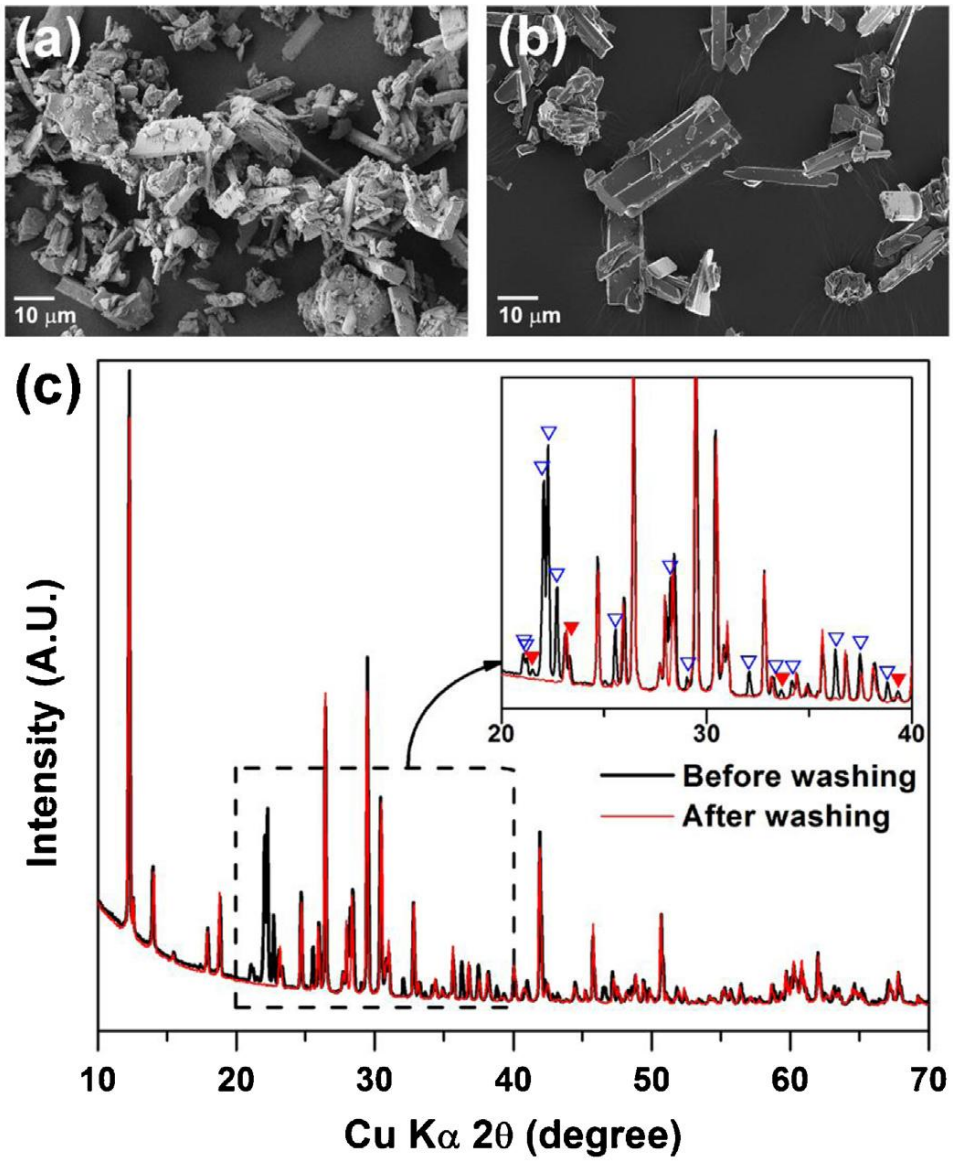

Fig. 3.2 SEM images of heat-treated samples at 600 ℃ for 10 h (a) before and (b) after washing with water. (c) XRD patterns of the heat-treated samples. Inset shows that reflections belong to the Li_2SO_4 (blue inverse triangle, PDF#04-012-7778) and that the $Li_2SO_4 \cdot H_2O$ (red inverse triangle, PDF#04-012-5077) is absent after washing. [89]

The sample prepared at 500 ℃ mainly consisted of $Li_{1.44}V_6O_{15}$ (β′ -$Li_xV_2O_5$ phase with $0.44 \leq x \leq 0.49$) and α-$Li_{0.04}V_2O_5$ with a small amount of LiV_3O_8 phase. For the sample that was heated-treated at 600 ℃, the α -$Li_{0.04}V_2O_5$ phase disappeared while the

β′-$Li_xV_2O_5$ remained as a main phase (c.a. 87 wt.%) with a small amount of LiV_3O_8 (c.a. 13 wt.%), as shown in Fig. 3.3. Table 3.1 also shows the structural information obtained from Rietveld refinement of the XRD patterns for the samples heat-treated in air at 600 ℃ and 700 ℃. The β′-$Li_xV_2O_5$ can be indexed based on a monoclinic structure with a space group of C2/m. Fig. 3.4 (b) illustrates the crystal structure of the β′-$Li_xV_2O_5$, which has a three dimensional tunneling structure along the [0 1 0] direction. Each Li+ ion in the β′- $Li_xV_2O_5$ ($0.44 \leq x \leq 0.49$) structure has fourfold coordination with oxygen ions, and its specific location is illustrated in Fig. 3.4 (b) insets. When the amount of Li slightly decreases in the β′-$Li_xV_2O_5$ phase, the β′ phase transforms to β-$Li_xV_2O_5$ phase ($0.22 \leq x \leq 0.37$), where Li+ ions have sevenfold coordination with oxygen ions [61, 78, 79].

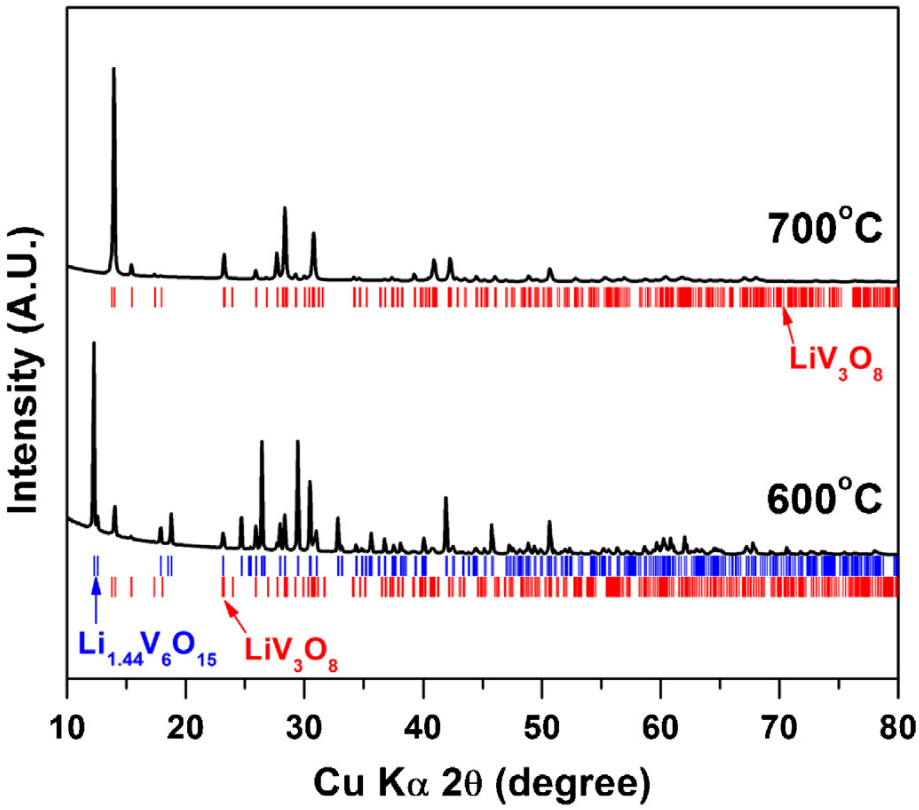

Fig. 3.3 XRD of the samples heat-treated at 600 ℃ and 700 ℃ for 10 h each and followed by washing with water. [89]

Table 3.1 : Structural parameters of powder samples obtained after heating in air at 600 ℃ and 700 ℃. [89]

Sample	Phases	Space group	a(A)	b (A)	c (A)	B (◦)	Unit cell volume (A^3)	Weight Fraction
600 ℃	$Li_{1.44}V_6O_{15}$ LiV_3O_8	C2/m $P2_1/m$	15.393 6.615	3.601 3.600	10.075 12.099	110.557 108.210	522.913 273.677	0.87 0.13
700 ℃	LiV_3O_8	$P2_1/m$	6.648	3.601	12.0390	107.821	274.383	1.00

The minor LiV_3O_8 phase observed in the 600 ℃ heat-treated samples can be indexed based on a monoclinic structure with a space group of P21/m. After further increasing the temperature to 700 ℃, the XRD showed that the resulting powder consisted of single LiV_3O_8 phase, as shown in Fig. 3.3. Table 3.1 lists the structural parameters of the LiV_3O_8 phases observed in the 600 ℃ and 700 ℃ heat-treated samples. Unlike the β′-$Li_xV_2O_5$, the LiV_3O_8 has a layer structure consisting of ribbons of 5- and 6-coordinated vanadium where the lithium atoms are located between two layers and linked by oxygen atoms (see Fig. 3.4 (c)).

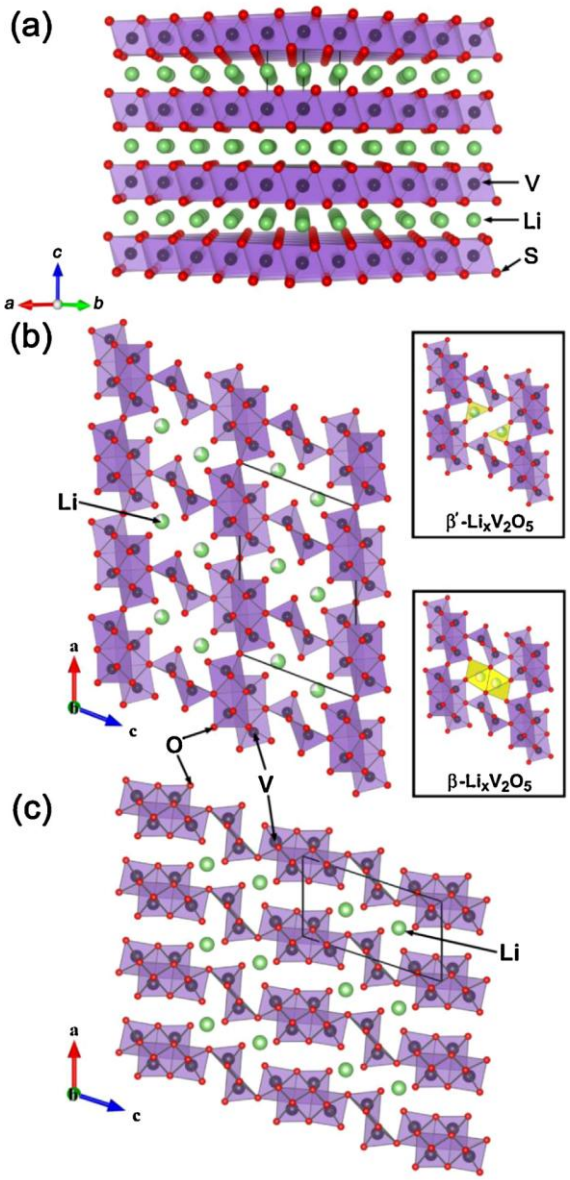

Fig. 3.4 Crystal structure of (a) layered $LiVS_2$, (b) three dimensional framework β′-$Li_xV_2O_5$ (insets illustrate different Li^+ locations between β′-phase and β –phase $Li_xV_2O_5$), and (c) layered LiV_3O_8. [89]

3.3.2 SEM, TEM and TOF SIMS Analyses of Heat-treated Sample

Fig. 3.5 shows SEM images of powder samples that were heat-treated in air at 600 ℃ and 700 ℃ and then subjected to the washing and drying processes. As is characteristic of the β′ -$Li_xV_2O_5$ phase, the 600 ℃ sample mainly consisted of well-

developed rod-shaped crystals that were approximately 20-30 μm in length and 3-6 μm in width, as can be seen in Fig. 3.5 (a) – (c). In contrast, the 700 ℃ sample consisted of agglomerations of fibers, as can be seen in Fig. 4.5 (d) – (f), which is a characteristic of the LiV_3O_8 phase.

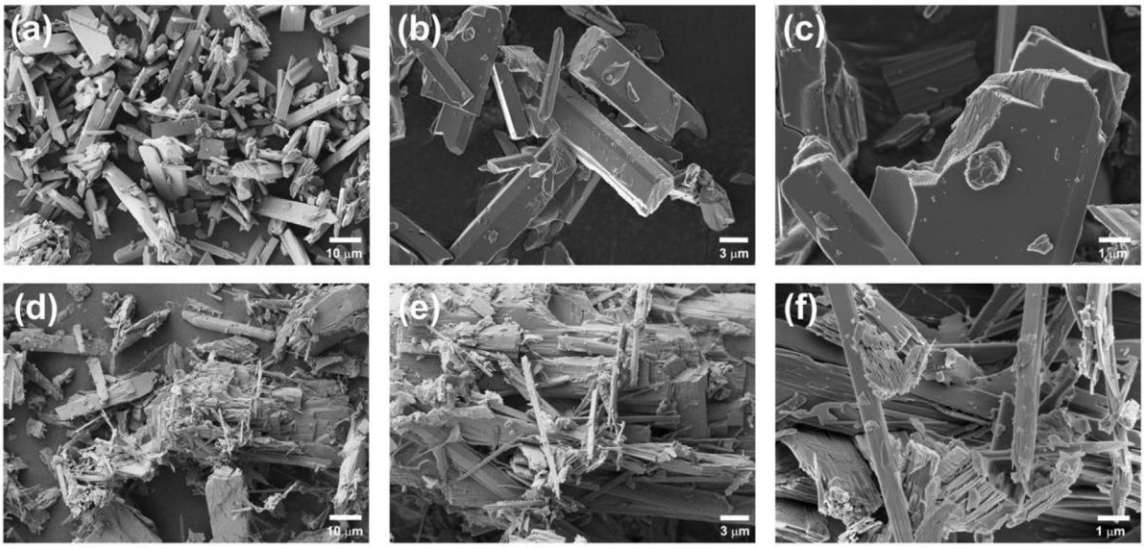

Fig. 3.5 The SEM micrograph of the $LiVS_2$ annealed at different temperatures for 10 h; (a-c) at 600 ℃, sample mainly consists of β′ -$Li_xV_2O_5$ with minor LiV_3O_8 phase; (d-f) at 700 ℃, sample consists of pure LiV_3O_8 phase. [89]

A higher magnification SEM image in Fig. 3.5 (c) shows that the rod-shaped crystal exposed layers of grains. TEM was used to further observe the structural characteristics of the layered grains in the bulk of the β′-$Li_xV_2O_5$. To determine the direction of the crystal growth on such layered grains, thin platelets were separated from the grains by grinding the rod-shaped crystals. As a result, TEM found that platelets were oriented in a "face-on" direction, as shown in Fig. 3.6 (a) , whereupon a high-resolution image was taken of them (see Fig. 3.6 (b)). It was determined from the fast Fourier transform (FFT) of the high-resolution image (see Fig. 3.6 (c)) that the normal orientation of the platelet is parallel to the [1 1 0] zone axis of β′ -$Li_xV_2O_5$. This indicates that the growth direction of the platelet is along the a-b atomic plane and normal to the c-axis direction (see Fig. 3.4 (b)). This is also supported by the platelet's calculated diffraction

pattern along the [1 1 0] zone axis using the Java version of the Electron Microscopy Simulation (JEMS) program.

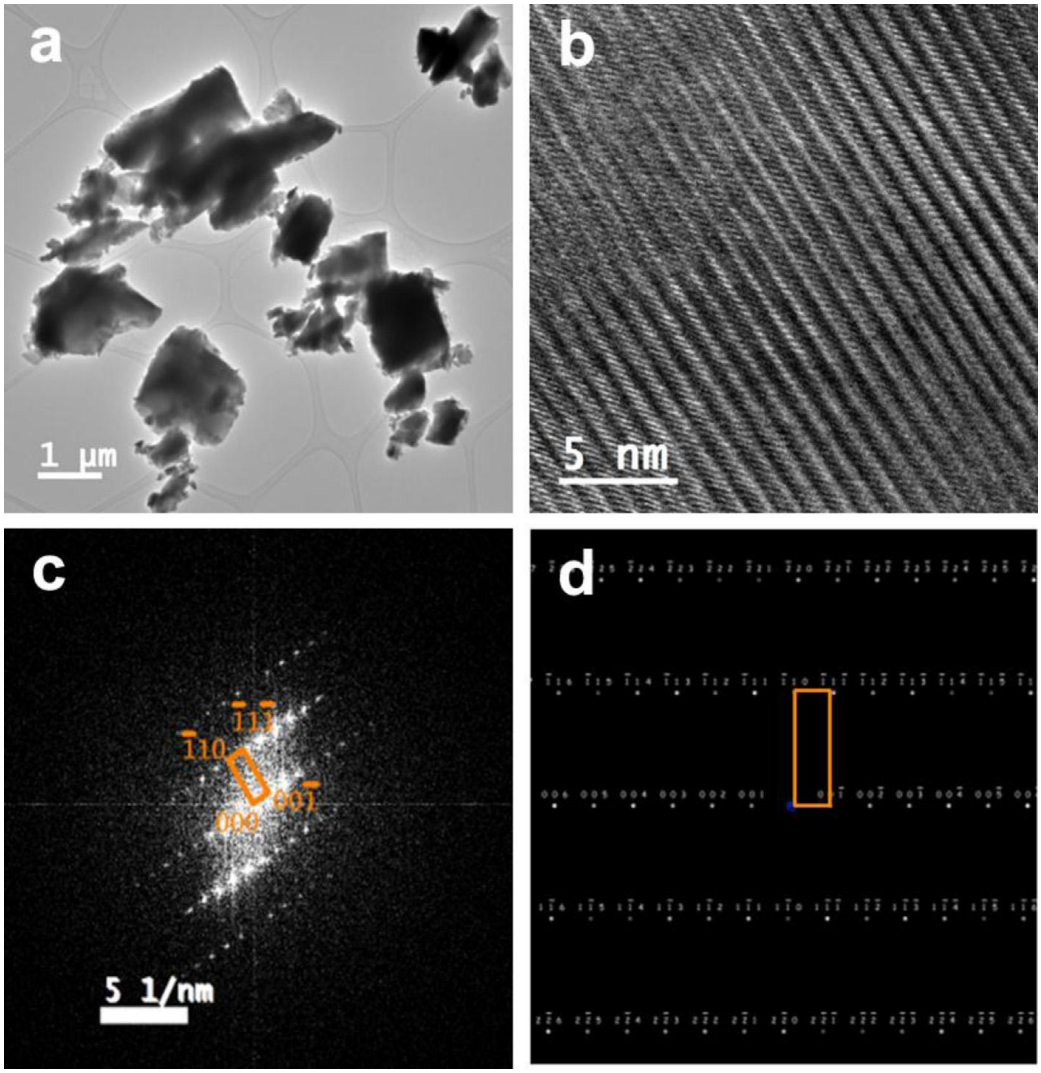

Fig. 3.6 (a) A typical TEM image of β′ –$LiVO_5$ particles having a platelet-like morphology. (b and c) A high-resolution TEM image of a platelet and its fast Fourier transform (FFT) pattern. It is determined from (b) and (c) that the normal of the platelet is parallel to the [1 1 0] zone axis of $Li_{1.44}V_6O_{15}$. This indicates the growth direction of the platelet is along the a and b atomic plane. (d) Calculated diffraction pattern of $Li_{1.44}V_6O_{15}$ along the [1 1 0] zone axis using the Java version of the electron microscopy simulation (JEMS) program. [89]

It is also interesting to note that high resolution TEM imaging revealed an amorphous film (~20 nm thick) on top of the β′ -$Li_xV_2O_5$ particle, of which the interface is marked with white dotted-lines in Fig. 3.7 (a). Elemental analysis of the amorphous film was performed by using both EDX and EELS techniques, which detected V, O, and a small trace of S. A trace amount of S element was also confirmed by the time-of-flight secondary ion mass spectroscopy (TOF SIMS) analysis shown in Fig. 3.7 (d), where two different measurement points were compared and showed different intensities between sulfur and oxygen elements. This TOF SIMS analysis implies that the chemical composition of the coating may differ at different sites in the sample. These measurements indicate that the amorphous film formed on the β′ -$Li_xV_2O_5$ surface mainly consists of V, O, and S elements. Li could also be a part of the amorphous film, but it could not have been identified from the above measurements. It could be expected that the vanadium oxysulfide amorphous phase formed during the phase evolution of the vanadium oxide from the vanadium sulfide. The vanadium oxysulfide amorphous phases such as V_2O_4S and V_2O_6S actually exist and were reported in the literature [90-92]. Further investigation is needed to elucidate the exact chemical compositions, formation mechanism, and role that the surface amorphous film has on enhanced electrochemical performance.

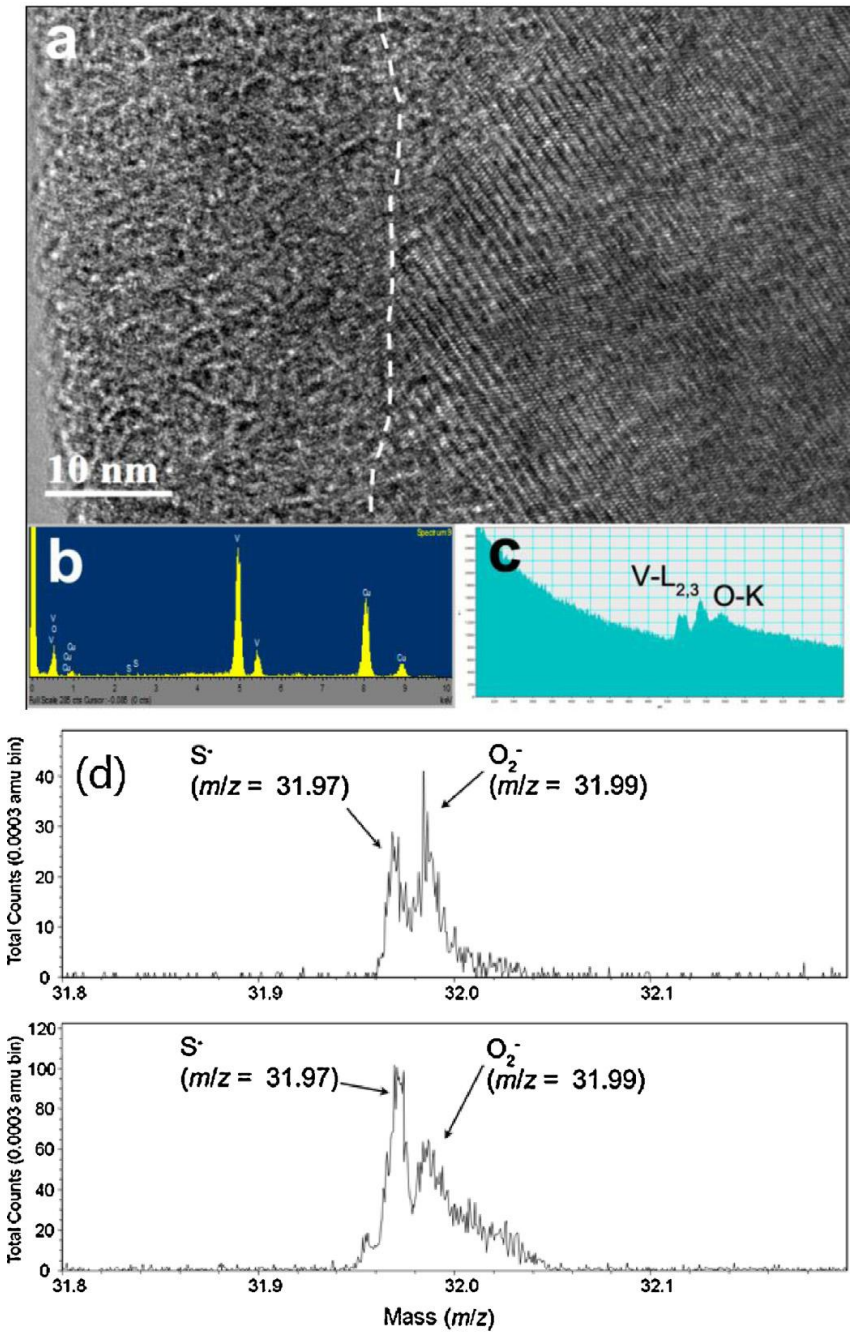

Fig. 3.7 (a) A high-resolution TEM image showing a platelet-like β′ -$Li_xV_2O_5$ particle. This platelet-like particle is coated with an amorphous film that is approximately 20 nm thick. (b) Energy-dispersive X-ray spectrometry (EDS) taken from the amorphous coating layer indicates that the amorphous layer contains V and O. The Cu signal is from the Cu TEM grid. (c) Electron energy loss spectroscopy (EELS) confirms that V and O are present in the amorphous layer, which is in agreement with EDS. (d) Secondary ion-mass spectrometry (SIMS) analysis for the β′ -$Li_xV_2O_5$ particle. [89]

3.3.3 Charge-discharge Voltage Curves of The Heat-treated Samples

In Fig. 3.8, the charge-discharge voltage curves of the samples prepared by heat-treating the pure $LiVS_2$ sulfide are shown and compared with that of the pure sulfide. Fig. 3.8 (a) shows that, by accessing the $V4^+/V3^+$ redox couple, the pure $LiVS_2$ sample has a specific capacity of ~180 mAh g^{-1} with reversible Li intercalation into its layered structure. The $LiVS_2$ sample's electrochemical potential versus Li metal is observed to be about 2.3 V, and its detailed electrochemical performance was already reported in the literature [70]. When the $LiVS_2$ sample was heated to temperatures of 500 ℃, 600 ℃, and 700 ℃, the voltage curve and range dramatically changed depending on the temperature. The second discharge curve of each sample is compared in Fig. 3.8 (d). It is evident that the voltage curves of the heat-treated samples are completely different from that of the mother sulfide sample. The voltage steps observed during the discharge of the sample correspond to the sample's phase change during Li insertion into the sample. Since there exist three phases, β'-$Li_xV_2O_5$, α-$Li_{0.04}V_2O_5$, and LiV_3O_8, in the 500 ℃ sample, and they are all electrochemically active during the discharge (Li insertion), the discharge voltage curve would be a combination of Li insertion into three phases. The discharge voltage curve observed from the 700 ℃ sample has a very typical voltage shape for the LiV_3O_8 phase, as reported in the literature [93, 94], which is also consistent with the XRD result observed in Fig. 3.3. For the 600 ℃ sample, the observed discharge voltage curve is more likely that of the β'-$Li_xV_2O_5$ phase that is reported in literature [78, 95], and its voltage curves and corresponding phase transformations are discussed in below.

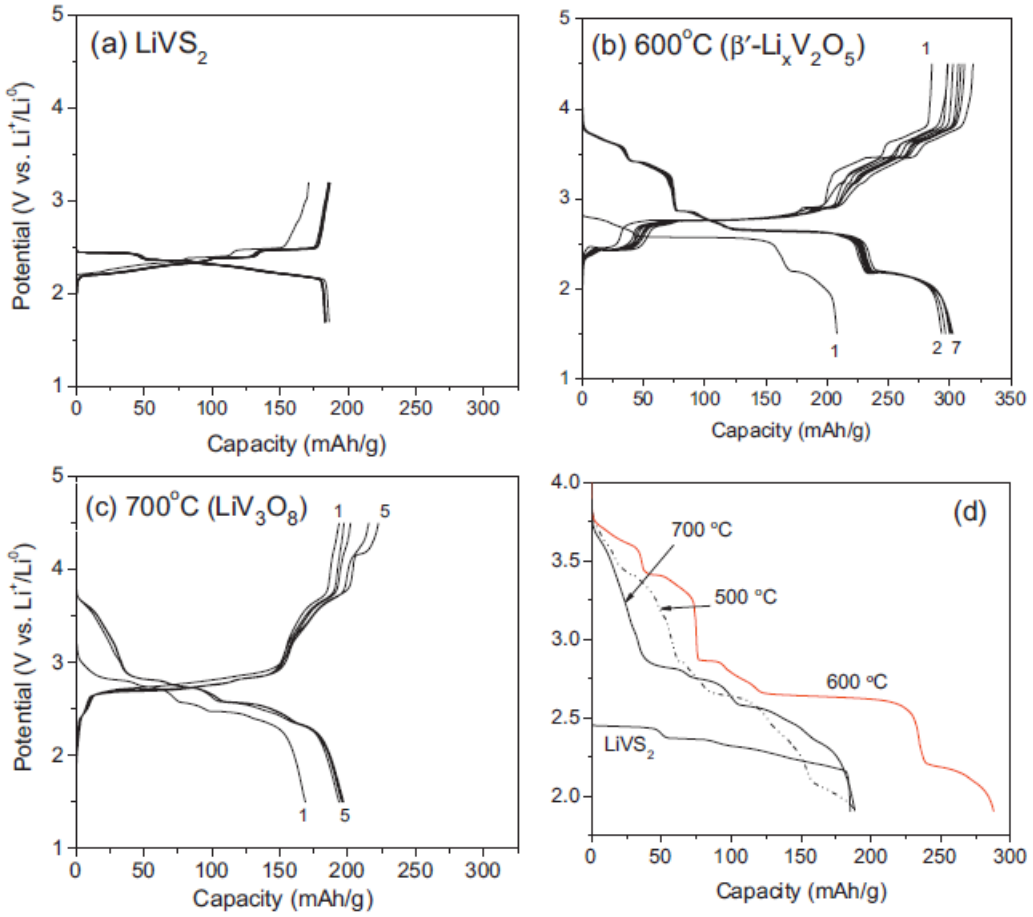

Fig. 3.8 Charge and discharge voltage curves of (a) the $LiVS_2$ sulfide sample and heat-treated at (b) 600 ℃ (β' -$Li_xV_2O_5$) and (c) 700 ℃ (LiV_3O_8), respectively. (d) Comparison of the second discharge voltage curves of the LiVS2, heat-treated at 500 ℃, 600 ℃, and 700 ℃. They were measured at the current rate of 0.2 mA/cm^2 (0.07 C). [89]

The sample prepared at 600 ℃ was charged first by extraction of Li from the sample, as can be seen in Fig. 3.9 (a). Two distinct charge voltage curves were observed in a range of 3.2 - 4.0 V during the first charge, and their corresponding specific capacities are ~67 mAh g^{-1}. Since the Li cannot be extracted from the LiV_3O_8 phase by oxidation of $V5^+$ to $V6^+$ [93, 94], the first charge voltage curve with the capacity of ~67 mAh g^{-1} corresponds to the extraction of ~0.49 Li from the β'-$Li_xV_2O_5$ (87 wt.%) phase in the 600 ℃ sample. The two distinct voltage curves observed at ~3.3 V and ~3.6 V

correspond to the formation of the β′ -$Li_xV_2O_5$ ($0.44 \leq x \leq 0.49$) and β-$Li_xV_2O_5$ ($0.22 \leq x \leq 0.37$), respectively, as indicated in Fig. 3.9 (a). This result is consistent with the data reported in the literature [78, 95]. These two distinct voltage curves are repeatable when discharging the cell between 4.0 V and 3.0 V.

When discharging the 600 ℃ sample, the minor LiV_3O_8 phase (13 wt.%) became electrochemically active by reduction of $V5^+$ to $V4^+$ with the insertion of Li into its structure. However, the discharge voltage curves of the LiV_3O_8 phase, which were observed in Fig. 3.8 (c), were not distinguishable from that of the 600 ℃ sample (Fig. 3.8 (b)). In addition, the distinct voltage steps observed in the 600 ℃ sample were clearly different from those observed in the LiV_3O_8 phase (Fig. 3.8 (d)). These voltage steps are very similar to those of the β′-$Li_xV_2O_5$ phase reported in literature [78, 95], which suggests that the 600 ℃ sample mainly represents a voltage profile of the β′-$Li_xV_2O_5$ phase. Hence, the voltage steps observed in the 600 ℃ sample mainly correspond to the phase transformations with Li insertion into the β′-$Li_xV_2O_5$ phase. All of these phase transformations were reversible during cycling between 1.5 V and 4.0 V.

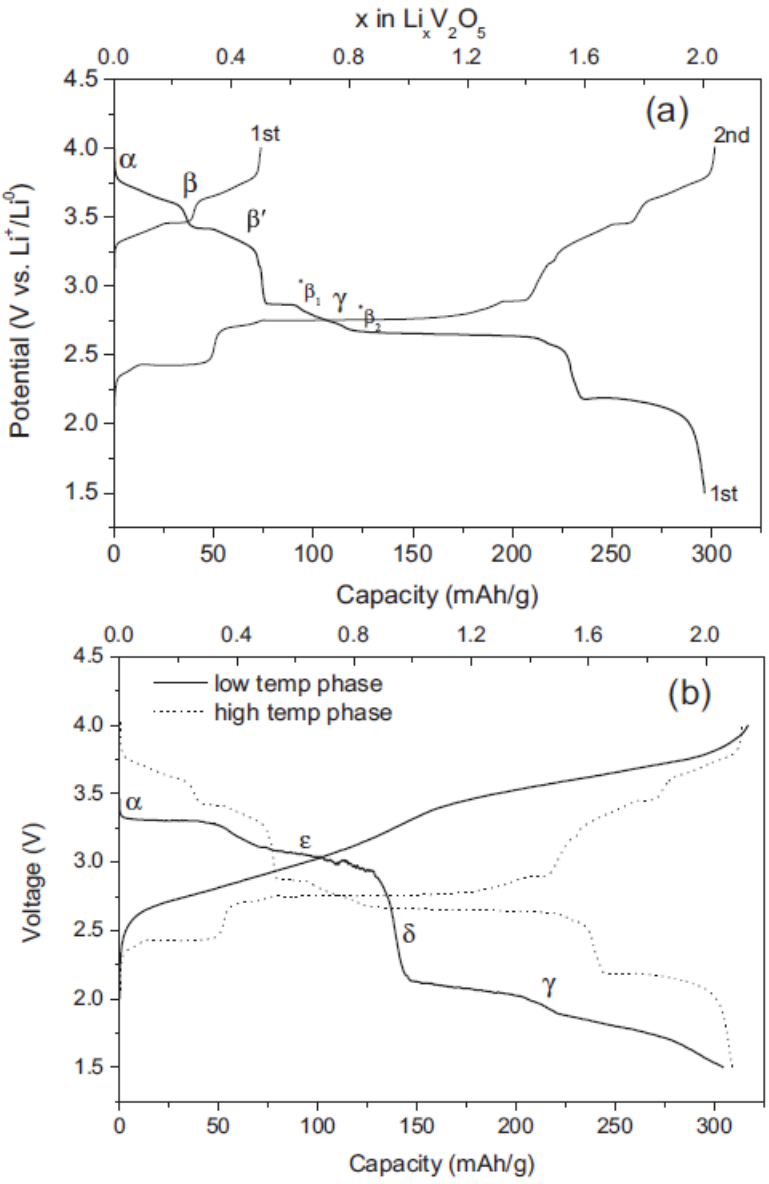

Fig. 3.9 Charge and discharge voltage curves of (a) a high temperature $Li_xV_2O_5$ phase and (b) a low temperature $Li_xV_2O_5$ phase, both measured at 0.2 mA/cm2 (0.07 C). (c) Phase diagram of the various homogeneity range of α, β, β′ , and γ phases for the high temperature $Li_xV_2O_5$ and α, ε, and γ phases for the low temperature $Li_xV_2O_5$, according to data provided by [9-11]. The voltage steps observed in the discharge voltage curves of (a) and (b) correspond to the phase transformations of the $Li_xV_2O_5$ with the electrochemical insertion of Li. [89]

3.3.4 Low Temperature vs. High Temperature $Li_xV_2O_5$ Phase

Fig. 3.9 (b) shows the first cycle of a low temperature (< 400 ℃) $Li_xV_2O_5$ phase in the 1.5 - 4.0 V electrochemical potential range. A series of discharge voltage steps observed in the low temperature $Li_xV_2O_5$ phase correspond well to the phase transformation during Li insertion reported in the literature [61, 78, 79]: α for $x \leq 0.1$, ε for $0.35 \leq x \leq 0.7$, δ for $0.9 \leq x \leq 1.0$, and additional γ and ω phases for $x > 1$. The phase transition from α - to δ -phase is fully reversible where $0 \leq x \leq 1$ in the low temperature $Li_xV_2O_5$. However, for $x > 1$, the structural transformation from the δ to γ phase is no longer reversible when the cell is discharged to below 2.2 V. This irreversible structural behavior was also illustrated in this work by the appearance of the irreversible charge voltage curve at a higher potential of approximately 3.0 V in Fig. 3.9 (b), which was reported to be the major cause for the poor cycle life of the low temperature $Li_xV_2O_5$ phase [53, 54].

In a high temperature (>400 ℃) $Li_xV_2O_5$ phase, four distinct crystal phases, α ($0 \leq x \leq 0.04$), β ($0.22 \leq x \leq 0.37$), β′ ($0.44 \leq x \leq 0.49$), and γ ($0.88 \leq x \leq 1$), were formed in the range of $0 \leq x \leq 1$ according to the phase diagram of the high temperature $Li_xV_2O_5$ phase [96]. It was also reported [96] that for $x > 1$, the additional Li insertion into γ - LiV_2O_5 caused the irreversible displacement reaction producing the V_2O_3 and $LiVO_3$ phases. However, Fig. 3.9 (a) shows that the electrochemical Li intercalation into the β′ - $Li_xV_2O_5$ is fully reversible in the range of $0 \leq x \leq 2$. The four distinct voltage steps observed above 2.6 V correspond to the formation of α, β, β′ and γ phases, respectively, but two additional reversible distinct voltage curves observed below 2.6 V did not correspond to the phase diagram reported in the literature.

The literature [78, 97] suggested that the phase transformations derived from the electrochemical Li insertion at room temperature could be different from the high temperature phase diagram. In addition to β and β′ phases, the formation of metastable phases such as β_1 ($x = 0.67$) and β_2 ($0.82 \leq x \leq 1.05$) was proposed whenever Li is electrochemically inserted into the tunnel structure of the β-$Li_xV_2O_5$ phase where three

types of Li sites exit. The literature also proposed [78, 97] that by the formation of the metastable phases, the maximum Li solubility for the β-$Li_xV_2O_5$ phase could be two (x = 2) by occupying all three Li sites in the structure. However, a full reversible electrochemical performance corresponding to Li intercalation in the range of $0.0 \leq x \leq 2.0$ was not reported in the literature.

This work shows that the electrochemical behavior of the β′ - $Li_xV_2O_5$ phase is fully reversible when $0 \leq x \leq 2$. This reversible electrochemical behavior is different from the high temperature phase diagram where the irreversible displacement reaction occurred in the high temperature $Li_xV_2O_5$ phase at $x > 1$, as suggested in the literature [96]. The ex situ XRD measurement was taken to investigate the phase transformation during the electrochemical Li intercalation into the β′-$Li_xV_2O_5$ phase when $0 \leq x \leq 2$, as shown in Fig. 3.10. Once electrochemically injecting Li, new broad peaks (consisting of several peaks) appeared at ~14 ° with the heights of the peaks growing during discharging of the cell. On the other hand, the main peaks corresponding to the β′ - $Li_xV_2O_5$ phase do not seem to change significantly during the discharging of the cell. Unfortunately, the quality of the XRD peaks was not clear enough to identify the structural transformation during the Li intercalation. Based on the current ex situ XRD data, it could be suggested that the main framework of the β′ -$Li_xV_2O_5$ structure may slightly change when the Li is electrochemically intercalated into its internal structure. A recent study of the β -$Na_{0.33}V_2O_5$ (having a similar structure to β′ -$Li_xV_2O_5$) also reported [98] that although the abrupt voltage steps were observed when the cell is cycled, the structure of the Li_xβ -$Na_{0.33}V_2O_5$ rarely changed during the electrochemical Li intercalation into the three types of Li sites in its structure when $0.0 \leq x \leq 1.66$. During the charging of the cell, the main XRD peaks indexed to the β′-$Li_xV_2O_5$ phase are recovered, as shown in Fig. 3.10. On the other hand, the new broad peaks at ~14 °, which appeared and grew during discharging of the cell, disappeared during charging of the cell. Unfortunately, the peaks at ~14 ° have not been identified at present. The in situ synchrotron X-ray diffraction measurement will be taken in a future study(s) to further

characterize structure changes of the β′ -LixV2O5 phase during electrochemical Li intercalation.

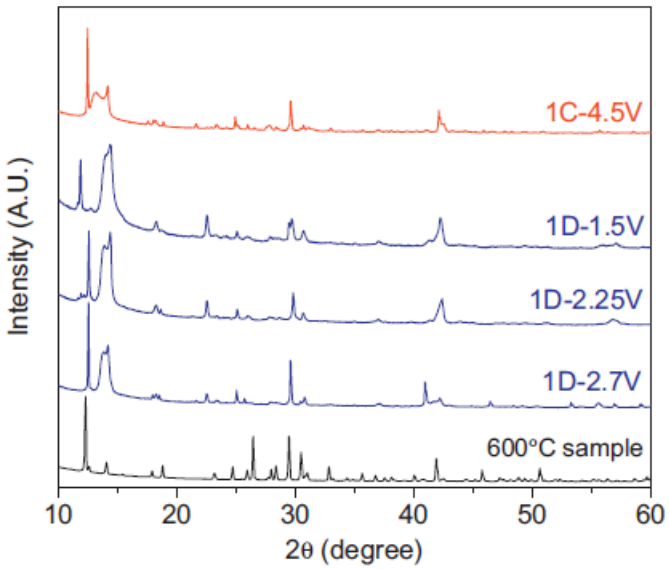

Fig. 3.10 The ex-suit XRD patterns of the 600 ℃ sample electrode during the first cycle: 1D: first discharge; 1 C: first charge. [89]

The cycle life of the high temperature β′ -$Li_xV_2O_5$ phase was tested in the 1.5 - 4.5 V range at different current rates, as shown in Fig. 3.11 (a). The discharge and charge capacity values slightly increased during the first few cycles. This could be due to the slight fragmentation of the micro-size grains induced by the electrochemical grinding, which was performed so that the smaller grain size could reduce the diffusion path for the Li ions and increase the battery's capacity. The discharge capacity reaches 310 mAh g^{-1} after five cycles at 0.2 mA/cm^2 (0.07 C) and fades to 276 mAh g^{-1} after 50 cycles, which yields 89% capacity retention. The discharge capacity decreases at higher current rates, but the capacity retention remains almost constant, 89% for 1.0 mA/cm^2 (0.4 C) and 88% for 4.0 mA/cm^2 (2.0 C). These cycle performances are promising when compared with the cycle life of the low temperature $Li_xV_2O_5$ phase (see Fig. 3.11 (a)) showing a poor

cycle performance at 0.2 mA/cm^2 (0.07 C), which is caused by the irreversible structural change from the δ to γ phase at $x > 1$ in $Li_xV_2O_5$. In the high temperature β′ - $Li_xV_2O_5$ phase, there is also an abrupt phase change from the layered α and γ phases to the three-dimensional β-based phases when $0 \leq x \leq 2$ during cycling. However, Fig. 3.11 (b) shows that the distinct voltage steps are repeatable during cycling even at higher C rates, which indicates that all phase transformations observed in the β′ -$Li_xV_2O_5$ phase are reversible during cycling when $0 \leq x \leq 2$.

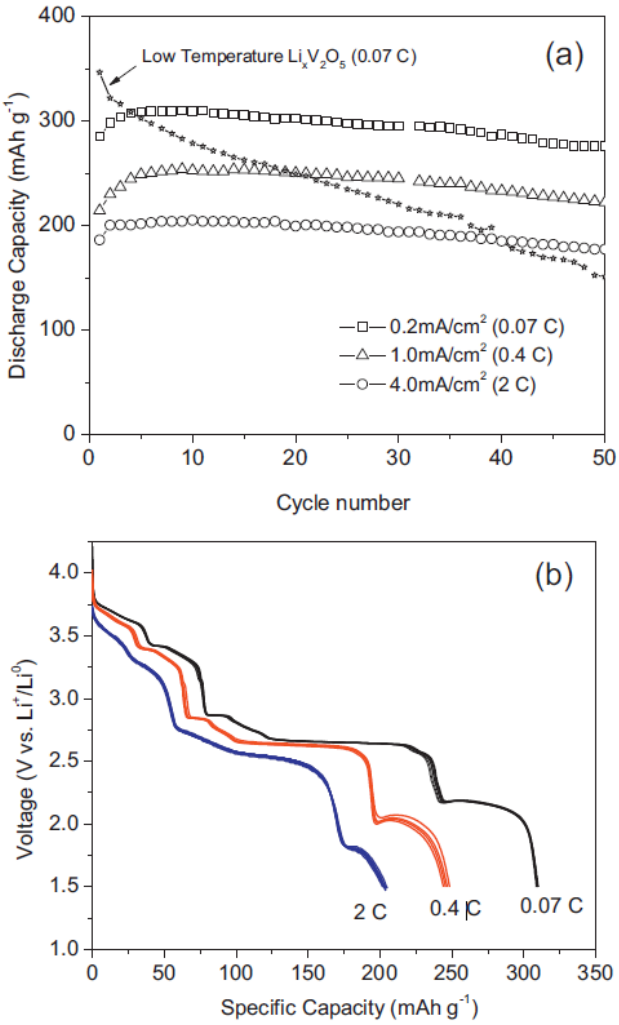

Fig. 3.11. (a) Cycle life performance of the 600 ℃ sample between 1.5 V and 4.5 V at the current rates of 0.2 mA/cm^2 (0.07 C), 1.0 mA/cm+ (0.4 C), and 4.0 mA/cm^2 (2 C), respectively, and compared with that of the low temperature sample between 1.5 V and 4.5 V measured at 0.1mA/cm^2 (0.07 C). (b) Discharge voltage curves of the 600 ℃ sample for the 5 cycles (5-10) measured at 0.07 C, 0.4 C, and 2 C, respectively. [89]

Three possible reasons can be expected for the phase reversibility of the β′ -$Li_xV_2O_5$ phase during cycling. First, the vanadium oxysulfide amorphous film coating on the surface of the β′ -$Li_xV_2O_5$ phase could stabilize the abrupt structural transformation during Li intercalation when cycling. Similar results were reported when V_2O_5 was

coated with carbon [72] and polypyrrole [73], showing improved cycle life. Second, the defects or impurities in the crystals, such as the sulfur left inside the structure, could possibly cause the formation of a β′ -$Li_xV_2O_5$-$_ySy$. Even a small amount (< 2%) of such an impurity could have a significant impact on the Li intercalation properties by stabilizing the structure. Examples include $M_{0.11}V_2O_{5.16}$ with M = $Al3^+$, $Fe3^+$, $Cr3^+$ [74-76]and $LiV_3O_{8-y}X$ (X = F, Cl) [77]. Third, the presence of the LiV_3O_8 phase as the second phase would have an impact on the phase reversibility of the β′ - $LixV_2O_5$ during cycling. A similar study of the $0.8LiV_3O_8–0.2V_2O_5$ composite [99] was recently reported, which showed that the composite's electrochemical performance was better than that of the bare LiV_3O_8 due to the presence of the V_2O_5 as the minor phase.

Since there are three possible reasons for the improved electrochemical performance of the 600 ℃ sample prepared in this work, it is challenging to determine which reason(s) is correct. We are planning a future research work to systematically study these three reasons and determine the clear mechanism of the reversible Li intercalation behavior of the β′ -$Li_xV_2O_5$ phase.

3.4 Conclusion

The β′ -$Li_xV_2O_5$ with high crystallinity was synthesized via a new chemical route, performing a chemical transformation from the vanadium sulfide to the vanadium oxide. Scanning electron microscopy (SEM) revealed rod-shaped powder morphology with particles 20-30 μm in length and 3-6 μm in width. In addition, the surface of the β′ - LiV_2O_5 particles was coated with an amorphous vanadium oxysulfide film (~20 nm thick). Unlike other reported $Li_xV_2O_5$ phases, the as-prepared β′ -$Li_xV_2O_5$ phase has a full a reversible insertion/extraction of two Li ($0 \leq x \leq 2$) per formula unit of $Li_xV_2O_5$, which corresponds to 310 mAh g^{-1} at a 0.07 C-rate in a voltage range of 1.5 - 4 V. Also, all of the phase transformations with electrochemical Li intercalation when $0 \leq x \leq 2$ were fully reversible from the layered structure of α and γ to the three-dimensional β-based structures.

The observed electrochemical performance of the high temperature β′ -LiV_2O_5 phase is promising when considering its large particle size and when compared with the performance of the low temperature $Li_xV_2O_5$ phase. Although this sample shows a relatively low voltage range compared with other cathodes such as $LiCoO_2$ (3.8 V) and $LiFePO_4$ (3.4 V), the large capacity of this sample is quite attractive in terms of increasing energy density in Li-ion batteries.

CHAPTER 4. REVERSIBLE $NAVS_2$ (DE) INTERCALATION CATHODE FOR NA-ION BATTERIES

4.1 Introduction

Cathode materials for Na-ion batteries that operate at room temperature have seen major advances in the last couple of years. Some of these examples are sodium layered oxides, poly-anionic materials, fluorides, framework oxides, NASICONs, and sulfate-fluorides [100, 101].There also exist various transition metal sulfides that can be employed in Na batteries. The early first-row transition metal layered sulfides possess suitable electrochemical properties, and the first work was directed primarily to binary metal sulfides, most notably, the prototype intercalation electrode, TiS_2 [102]. The Ti(IV)/(III) redox couple is about 1.8–2.0 V vs. Na. The layered TiS_2 provides soft bonding of Na to the sulfide atoms in the layers, and large gallery space between the TM layer slabs to fit Na+, which allows facile reversible electrochemical (de)intercalation. The electrochemical properties of other disulfides such as VS_2, TaS_2, ZrS_2, NbS_2 were elaborated by Abraham et al. [103], but in these cases, because of the molten-salt nature of the electrolytes, these electrodes were operated at moderate 130◦C. Herein, we report for the first time the room-temperature insertion/extraction of Na from $NaVS_2$ in order to evaluate the feasibility of the material as a cathode for Na-ion batteries. The structural change of Na_xVS_2 is monitored as a function of Na content, and the stable room-temperature phase of $NaVS_2$ is determined.

4.2 Experimental Method

For synthesis of $NaVS_2$, appropriate amounts of Na_2S (Aldrich), S (Alfa, 99.999%), and V (Aldrich, 99.5%) were mixed together in an Ar glove box and placed in

a carbon-coated quartz tube that was then sealed under vacuum. The tube was heated slowly over 20 h to 750 ℃, held for three days, and then cooled slowly over 5 h to 250 ℃, followed by quenching in air. The sample was removed from the tube in an Ar glovebox where it was thoroughly ground and pelletized. Then it was treated again at the same temperature with the same experimental process. Since this compound is moisture-sensitive, it was always handled in an Ar or He atmosphere. The electrode disks and cells were prepared in an Ar glove box. The electrodes were fabricated from a 70:20:10 (wt%) mixture of active material : acetylene black as current conductor : polytetrafluoroethylene as binder. Using 1M NaClO4 in ethylene carbonate/diethylene carbonate (1:1) as an electrolyte, the metal Na electrochemical half-cells (size 2032) were constructed as previously published [104].

The typical electrode mass and thickness were 5–10 mg and 0.03–0.08 mm. For powder X-ray diffraction (XRD), the prepared sample was finely ground and placed in the sample holder of the diffractometer (Bruker D8 Advance, Cu Kα) and then was sealed with thin amorphous Kapton tape inside the Ar glove box. For the ex-situ XRD measurements the cells were discharged or charged to a certain voltage and then disassembled in a Ar glove box, wherein the electrodes were washed with dry dimethyl carbonate (DMC). The dried electrodes were mounted on the XRD holder and sealed with Kapton tape for XRD measurements.

4.3 Result and Discussion

Na_xMS_2 with M = 1st row transition metal has the structure consisting of hexagonal-close-packed sulfur with M and Na ions in alternate octahedral-site (001) plane. On removal of Na, the MS_2 layers are held together by van derWaals bonding. Various phases of layered Na_xMS_2 have been reported according to the types of the sulfur packing and the sodium ion coordination being octahedral (O) or trigonal prismatic (P). Among them, the schematic diagram of O3-, P3-, and O1-type layered structures are

presented in Fig. 4.1. The letter O or P and following number indicates, respectively, the Na ion coordination geometry and number of $(MS_2)_n$ sheets in the unit cell.

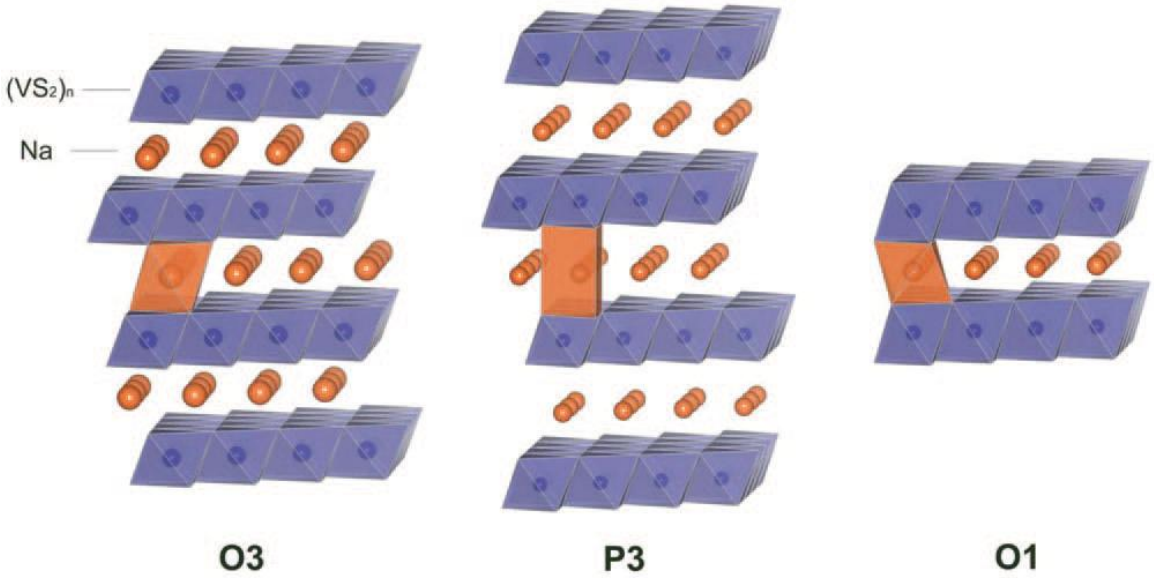

Figure 4.1 Schematic diagram of O3-, P3-, and O1-type layered structures. [69]

The structure of Na_xVS_2 was first reported by Wiegers et al. [68] They prepared Na_xVS_2 samples with various x values by heating the elements at 600 ℃ for four days in evacuated tube followed by quenching. In their experiment, the quenched Na_xVS_2 sample with $0.3 < x < 1.0$ had the P3-type structure (a = 3.346 Å and c = 21.02 Å) initially, but a slow phase transition from the P3- to O1- type structure was observed when the sample was stored at room temperature for an extended period of time. Accordingly, the authors assigned the P3- and O1- type structures as the high and low temperature phases of Na_xVS_2 ($0.3 < x < 1.0$), respectively. However, this assignment of the stable phases to Na_xVS_2 compounds is not conclusive since the authors also commented in the same paper that O3- phase (a = 3.566 Å and c = 19.68 Å) was frequently observed in some of their $NaVS_2$ samples as a second phase or even as a single phase. This indicated that the structure of Na_xVS_2 is sensitive to the sample preparation and handling condition: a high

temperature synthesis commonly gives sodium deficient layered chalcogenide compounds, and $NaVS_2$ is so reducing even at room temperature that it could readily react with CO_2 in the environment to form Na_2CO_3 on the surface of $NaVS_2$ particles [105, 106]. Because of these difficulties, the actual Na content in a synthesized $NaVS_2$ product may vary from sample to sample, and the determination of stable structure of $NaVS_2$ has not been conclusive. Our as-prepared $NaVS_2$ sample, which is also found to be Na-deficient from electrochemical analysis, presents both O3- and P3- type phases by X-ray diffraction, as seen in Fig. 4.2 (b) (bottom pattern (1)). The complex XRD pattern is fitted and indexed with both O3- and P3- type phases by Le Bail whole-powder pattern decomposition method. [107]

Figure 4.2 (a) displays the voltage profile curve of a Na_xVS_2 electrode cycled between 1.3–3.1 V at room temperature. When the electrochemical cycle is started with a discharge process, the voltage profile curve shows a plateau at ca. 1.7 V and then a rapid drop until the voltage reaches the 1.3 V cutoff value. This voltage response, which is seen repeatedly in the following discharge curves, is associated with the electrochemical Na-insertion to the octahedral vacancies in Na layers of Na_xVS_2 to form $NaVS_2$. This confirms that the fresh electrode material is Na-deficient Na_xVS_2. The amount of Na electrochemically inserted to the fresh Na_xVS_2 electrode during the first discharge is ~0.3 mole per formula unit corresponding to $x \sim 0.7$ for the fresh Na_xVS_2 electrode. The subsequent charge-discharge cycle of Na/Na_xVS_2 cell in Fig. 4.2 (a) shows a reversible voltage profile with the specific capacity close to the theoretical value of 194 mAh/g, proving that Na can be reversibly cycled with Na_xVS_2 in the range of $0 < x < 1$ at room temperature. The voltage slopes and corresponding ex-situ XRD patterns, shown in Fig. 4.2 (a) and 4.2 (b), identify the room-temperature solid-solubility ranges of the O3-, P3-, and O1- type phases. Accordingly, the successive flat voltage regions represent the two-phase regions of O3 + P3 and P3 + O1 phases, and the room temperature phase diagram of Na_xVS_2 as a function of Na content, x is constructed as in Fig. 4.2 (a). Because of the highly reducing nature of O3-$NaVS_2$, the as-prepared $NaVS_2$ samples may easily decompose to Na-deficient Na_xVS_2 form during the high-temperature synthesis and

subsequent sample handling process. Therefore, at the point of analysis, the samples could have been transformed to P3 + O3 phases or to a single P3-phase according to the degree of decomposition and consequent x value.

Figure 4.2 (c) shows the plot of capacity retention for the Na/Na_xVS_2 cell cycled between 1.3–2.5 V. The cell was discharged first and the subsequent charge-discharge cycle was designated as 2nd cycle. The specific discharge capacity at the 2nd cycle is 155 mAh/g, and 75% of the initial discharge capacity is retained at 30th cycle. The observed capacity degradation may be related to a local structural change of $NaVS_2$ or parasitic reaction between $NaVS_2$ and electrolyte, which could build up a thick SEI layer on the surface of cathode. The succeeding voltage profiles of selected cycle numbers (inset of Fig. 4.2 (c) shows characteristic shape features that are similar to the initial voltage profile indicating a highly reversible layer gliding. This result is particularly interesting since its oxide counterpart, Na_xVO_2, is only possible to be reversibly cycled in the range of $0.5 < x < 1.0$, at room temperature [105]. A monoclinic distortion of O3-$NaVO_2$ is observed upon Na-deintercalation to $Na_{0.5}VO_2$, and the layered structure is not maintained at further Na-deintercalation below $x = 0.5$ exhibiting significant amorphization. The high electrochemical utilization of Na ions in Na_xVS_2 is associated with high covalency in $(VS_2)n$ host lattice, which reduces the electrostatic repulsion between two adjacent $(VS_2)n$ slabs [108]. Therefore, as a result of reversible layer gliding, Na_xVS_2 can maintain layered structure even at a very low Na content (i.e. $x < 0.5$) where Na is not tightly bound.

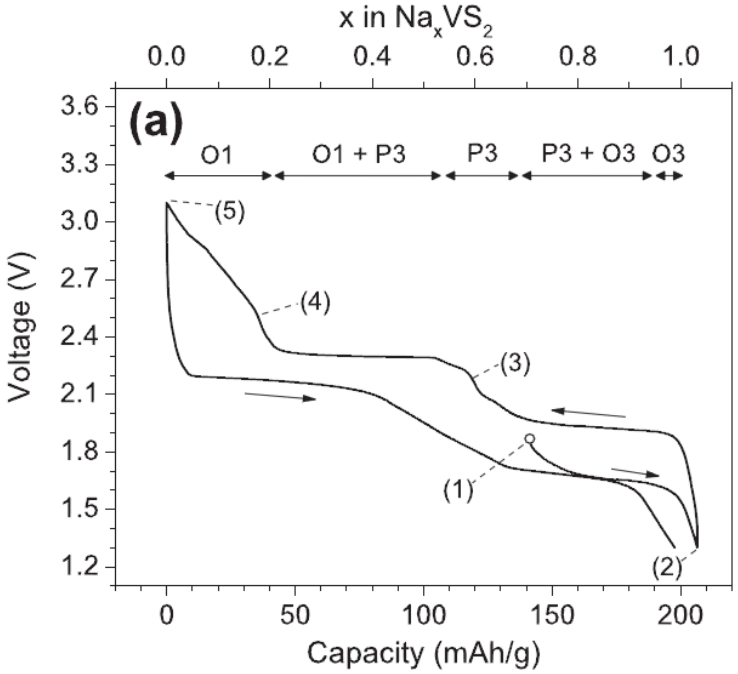
x in Na_xVS_2
0.0
0.2
0.4
0.6
0.8
1.0
(a)
O1
O1 + P3
P3
P3 + O3
O3
(5)
(4)
(3)
(2)
(1)
Voltage (V)
3.6
3.3
3.0
2.7
2.4
2.1
1.8
1.5
1.2
0
50
100
150
200
Capacity (mAh/g)

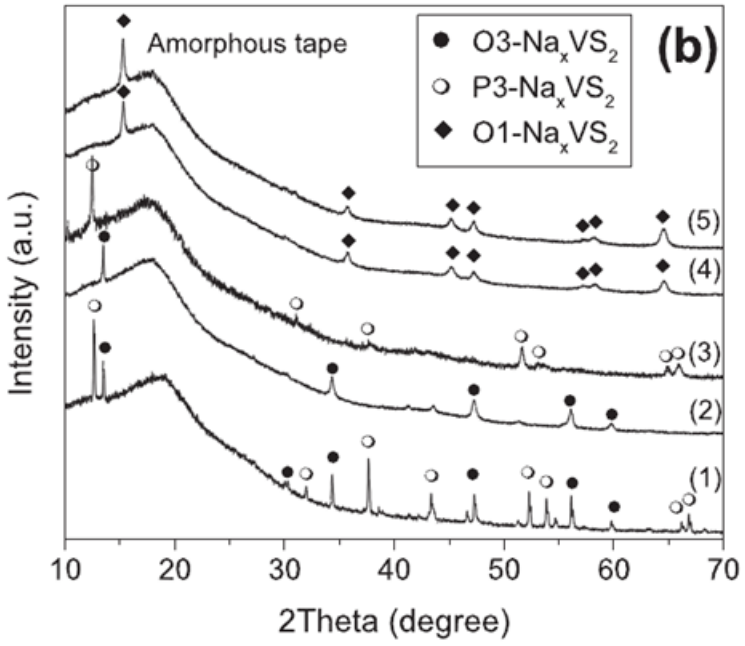
Amorphous tape
O3-Na_xVS_2
P3-Na_xVS_2
O1-Na_xVS_2
(b)
(5)
(4)
(3)
(2)
(1)
Intensity (a.u.)
10
20
30
40
50
60
70
2Theta (degree)

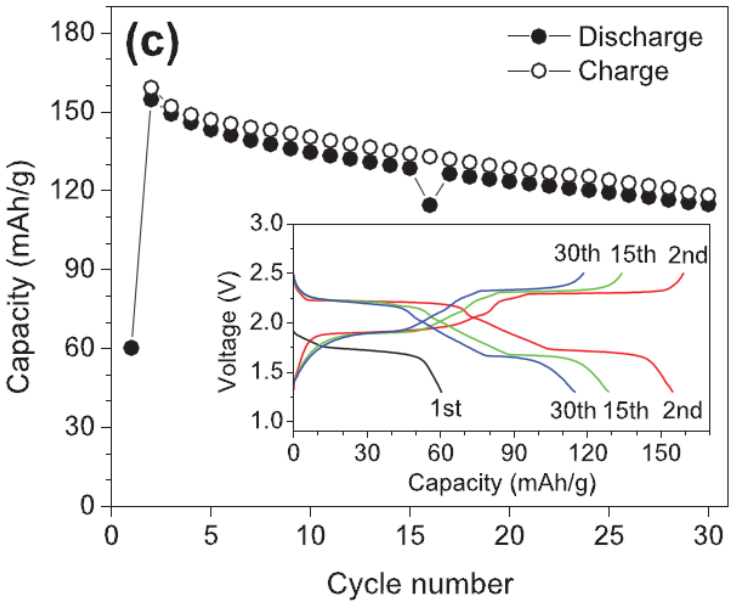

Figure 4.2 (a) Voltage profile of the Na/Na_xVS_2 cell cycled with 1 M $NaClO_4$ in EC:DEC (1:1) electrolyte between 1.3–3.1 V at the rate of 15 mA/g, (b) ex-situ XRD patterns of the cycled electrode at the designated voltages: (1) starting phase, (2) discharged to 1.3 V, (3) charged to 2.2 V, (4) charged to 2.5 V, and (5) charged to 3.1 V, and (c) capacity retention of the Na/Na_xVS_2 cell cycled between 1.3–2.5 V at the rate of 15 mA/g. The inset of (c) shows the voltage profiles of selected cycles. [69]

4.4 Conclusion

We have shown that reversible electrochemical deintercalation of x ~ 1.0 Na per formula unit of Na_xVS_2, corresponding to a capacity of ~200 mAh/g, is possible, and a stable capacity of ~ 120 mAh/g after 30 cycles is observed. A room-temperature phase diagram of Na_xVS_2 ($0 < x < 1$) has been constructed by monitoring cell potential as a function of Na content, x during the deintercalation, and the stable phase for $NaVS_2$ was determined as O3-type structure. While Na_xVS_2 shows O3-, P3-, and O1-type phase transition during the whole range of deintercalation from x = 1.0 to x = 0, more stable performance could be achieved when the material is cycled out of the single O1 phase region. Therefore, further research on the correlation between structure and electrochemical property of this family of materials is required for better understanding.

CHAPTER 5. CONCLUSIONS AND FUTURE WORK

5.1 Conclusion

Further development is still needed for other applications of lithium ion rechargeable batteries, for example, transportation. With the performance of current batteries, a large number are needed in order to provide energy equivalent to a gallon of gas. Not only that, but the energy density of lithium ion batteries also needs to be improved for future devices as the technology advances. In order to do that, increasing the performance of electrodes, especially cathode materials, is one of the approaches to improve the energy density of batteries. High operation voltage is one of the factors that determine the performance of cathode material. The cell voltage is affected not only by the difference in the work functions of the cathode and anode, but also by the crystal structure and the coordination geometry of the sites into/from which the Li+ ions are inserted/extracted. Other than that, another important characteristic for cathode materials are safety, capacity, life cycle, cost and environmental compatibility.

According to the first chapter, Vanadium pentoxide, V_2O_5 has a high theoretical capacity of 442 mAh/g. However, due to the irreversible structural change when Li insertion is more than x = 1, the practical reversible capacity of vanadium pentoxide has been limited. Effort to improve the phase reversibility of $Li_xV_2O_5$ has been made. Vanadium pentoxide's structure, surface defects, and morphology can be changed using different method of synthesis and post-treatment conditions. One of the synthesis methods is to dope Na into V_2O_5, and then heat-treatment to form $NaVS_2$ sulfide. Significant morphology changes were observed during the treatment such as the formation rod-shaped particles and particle size increases. Best performance was

obtained with 600 ℃ of heat-treatment with capacity of 265 mAh/g at 0.1 mA/cm^2. The result seems to be promising, and further studies need to be done for suitable application.

From the fourth chapter, fully reversible Na-intercalation was found with $NaVS_2$ as cathode material in Na-ion battery. Similar to lithium ion battery, fully reversible Li intercalation observed at $0 < x < 2$. During the change and discharge process, the structure of $NaVS_2$ changed from phase O1 , O1 + P3 , P3, P3 + O3 , O3 and gradually changed back to the O1 phase during opposite process. Due to this phenomenon, $NaVS_2$ is being categorized as "smart material" because it could change back to its original structure once it is deformed during charge or discharge process. This is very rare for most of cathode materials as it is very difficult for the material structure to change back to its original structure once deformed. Although this cathode material shows some promising results, more research needed to be done on determine a stable structure of $NaVS_2$.

5.2 Future Work

Vanadium pentoxide shows some promising performance as a new cathode material for lithium ion batteries and sodium ion batteries. There are several methods to achieve this material such as various ways of synthesizing and post-treatment method. New chemical approaches and heat-treatment are being used to change its structure and morphology which lead to better performance in terms of energy density, capacity and cycle life. Although this cathode material has a relatively low voltage range compared with other commercial cathodes, it could serve as an alternative cathode material for the future due to its large capacity and increasing energy density. Further development of vanadium pentoxide are required to ensure a safe, low-cost and high power density cathode as the next generation power source.

For future development, research on nanotechnology should be applied to vanadium pentoxide. Currently, nanotechnology is a very popular field due to its

characteristics. Comparing a bulk material and nano-sized particles, nanoparticles provide large surface areas for reaction. Researchers should develop different synthesis methods and heat-treatment method to manufacture nanoparticle vanadium pentoxide for rechargeable lithium ion batteries. With the application of nanotechnology, lithium ion batteries might provide a much larger power density and energy density, longer cycle life, lighter weight or even faster charging and discharging rate. If these characteristic were to be implemented on to rechargeable lithium ion batteries, the size of batteries on electronic devices could be reduced significantly without losing performance. This will definitely provide convenience towards the user of electronic devices.

LIST OF REFERENCES

LIST OF REFERENCES

[1] J. B. Goodenough and Y. Kim, "Challenges for Rechargeable Li Batteries†," *Chemistry of Materials,* vol. 22, pp. 587-603, 2009.

[2] B. Garcia, S. Lavall ée, G. Perron, C. Michot, and M. Armand, "Room temperature molten salts as lithium battery electrolyte," *Electrochimica Acta,* vol. 49, pp. 4583-4588, 2004.

[3] R. Moshtev and B. Johnson, "State of the art of commercial Li ion batteries," *Journal of power sources,* vol. 91, pp. 86-91, 2000.

[4] P. G. Bruce, B. Scrosati, and J. M. Tarascon, "Nanomaterials for rechargeable lithium batteries," *Angewandte Chemie International Edition,* vol. 47, pp. 2930-2946, 2008.

[5] D. H. Jang, Y. J. Shin, and S. M. Oh, "Dissolution of Spinel Oxides and Capacity Losses in 4 V Li/Li x Mn2 O 4 Cells," *Journal of The Electrochemical Society,* vol. 143, pp. 2204-2211, 1996.

[6] I. Stassen and G. Hambitzer, "Metallic lithium batteries for high power applications," *Journal of power sources,* vol. 105, pp. 145-150, 2002.

[7] G. Halpert, "Past developments and the future of nickel electrode cell technology," *Journal of power sources,* vol. 12, pp. 177-192, 1984.

[8] E. Markevich, V. Baranchugov, and D. Aurbach, "On the possibility of using ionic liquids as electrolyte solutions for rechargeable 5V Li ion batteries," *Electrochemistry communications,* vol. 8, pp. 1331-1334, 2006.

[9] M. S. Whittingham, "Lithium batteries and cathode materials," *Chemical Reviews,* vol. 104, pp. 4271-4302, 2004.

[10] A. Nishimoto, M. Watanabe, Y. Ikeda, and S. Kohjiya, "High ionic conductivity of new polymer electrolytes based on high molecular weight polyether comb polymers," *Electrochimica acta,* vol. 43, pp. 1177-1184, 1998.

[11] T. Ohzuku, Y. Iwakoshi, and K. Sawai, "Formation of Lithium-Graphite Intercalation Compounds in Nonaqueous Electrolytes and Their Application as a Negative Electrode for a Lithium Ion (Shuttlecock) Cell," *Journal of The Electrochemical Society,* vol. 140, pp. 2490-2498, 1993.

[12] Y. Koyama, N. Yabuuchi, I. Tanaka, H. Adachi, and T. Ohzuku, "Solid-State Chemistry and Electrochemistry of $LiCo_{1/3}Ni_{1/3}Mn_{1/3}O_2$ for Advanced Lithium-Ion Batteries I. First-Principles Calculation on the Crystal and Electronic Structures," *Journal of The Electrochemical Society,* vol. 151, pp. A1545-A1551, 2004.

[13] T. Ohzuku and R. J. Brodd, "An overview of positive-electrode materials for advanced lithium-ion batteries," *Journal of Power Sources,* vol. 174, pp. 449-456, 2007.

[14] G. Amatucci and J.-M. Tarascon, "Optimization of Insertion Compounds Such as $LiMn_2O_4$ for Li-Ion Batteries," *Journal of The Electrochemical Society,* vol. 149, pp. K31-K46, 2002.

[15] K. Ariyoshi, Y. Iwakoshi, N. Nakayama, and T. Ohzuku, "Topotactic Two-Phase Reactions of Li $[Ni_{1/2}Mn_{3/2}]O_4$ (P4332) in Nonaqueous Lithium Cells," *Journal of The Electrochemical Society,* vol. 151, pp. A296-A303, 2004.

[16] A. K. Padhi, K. Nanjundaswamy, and J. B. d. Goodenough, "Phospho-olivines as Positive-Electrode Materials for Rechargeable Lithium Batteries," *Journal of the Electrochemical Society,* vol. 144, pp. 1188-1194, 1997.

[17] H. Huang, S.-C. Yin, and L. s. Nazar, "Approaching theoretical capacity of $LiFePO_4$ at room temperature at high rates," *Electrochemical and Solid-State Letters,* vol. 4, pp. A170-A172, 2001.

[18] N. Ravet, J. Goodenough, S. Besner, M. Simoneau, P. Hovington, and M. Armand, "Abstract# 127," in *196th Meeting of the Electrochem. Soc*, 1999.

[19] F. Croce, R. Curini, A. Martinelli, L. Persi, F. Ronci, B. Scrosati, *et al.*, "Physical and chemical properties of nanocomposite polymer electrolytes," *The Journal of Physical Chemistry B,* vol. 103, pp. 10632-10638, 1999.

[20] A. Pradel and M. Ribes, "Lithium chalcogenide conductive glasses," *Materials chemistry and physics,* vol. 23, pp. 121-142, 1989.

[21] L. Persi, F. Croce, and B. Scrosati, "A $LiTi_2O_4$–$LiFePO_4$ novel lithium-ion polymer battery," *Electrochemistry communications,* vol. 4, pp. 92-95, 2002.

[22] A. Dey and B. Sullivan, "The electrochemical decomposition of propylene carbonate on graphite," *Journal of The Electrochemical Society,* vol. 117, pp. 222-224, 1970.

[23] C. K. Chan, H. Peng, G. Liu, K. McIlwrath, X. F. Zhang, R. A. Huggins, *et al.*, "High-performance lithium battery anodes using silicon nanowires," *Nature nanotechnology,* vol. 3, pp. 31-35, 2007.

[24] F. Ronci, P. Reale, B. Scrosati, S. Panero, V. Rossi Albertini, P. Perfetti, *et al.*, "High-Resolution In-Situ Structural Measurements of the $Li_{4/3}Ti_{5/3}O_4$ "Zero-Strain" Insertion Material," *The Journal of Physical Chemistry B,* vol. 106, pp. 3082-3086, 2002.

[25] W.-J. Zhang, "A review of the electrochemical performance of alloy anodes for lithium-ion batteries," *Journal of Power Sources,* vol. 196, pp. 13-24, 2011.

[26] M. Egashira, H. Takahashi, S. Okada, and J.-i. Yamaki, "Measurement of the electrochemical oxidation of organic electrolytes used in lithium batteries by microelectrode," *Journal of power sources,* vol. 92, pp. 267-271, 2001.

[27] K. Hayashi, Y. Nemoto, S.-i. Tobishima, and J.-i. Yamaki, "Mixed solvent electrolyte for high voltage lithium metal secondary cells," *Electrochimica Acta,* vol. 44, pp. 2337-2344, 1999.

[28] X. Zhang, R. Kostecki, T. J. Richardson, J. K. Pugh, and P. N. Ross, "Electrochemical and Infrared Studies of the Reduction of Organic Carbonates," *Journal of The Electrochemical Society,* vol. 148, pp. A1341-A1345, 2001.

[29] H. Ye, J. Huang, J. J. Xu, A. Khalfan, and S. G. Greenbaum, "Li ion conducting polymer gel electrolytes based on ionic liquid/PVDF-HFP blends," *Journal of the Electrochemical Society,* vol. 154, pp. A1048-A1057, 2007.

[30] C. Sirisopanaporn, A. Fernicola, and B. Scrosati, "New, ionic liquid-based membranes for lithium battery application," *Journal of Power Sources,* vol. 186, pp. 490-495, 2009.

[31] J. Cho and M. Liu, "Preparation and electrochemical properties of glass-polymer composite electrolytes for lithium batteries," *Electrochimica acta,* vol. 42, pp. 1481-1488, 1997.

[32] K. Xu, "Nonaqueous liquid electrolytes for lithium-based rechargeable batteries," *Chemical reviews,* vol. 104, pp. 4303-4418, 2004.

[33] R. Imhof and P. Nov á k, "Oxidative Electrolyte Solvent Degradation in Lithium-Ion Batteries: An In Situ Differential Electrochemical Mass Spectrometry Investigation," *Journal of The Electrochemical Society,* vol. 146, pp. 1702-1706, 1999.

[34] R. Fong, U. von Sacken, and J. Dahn, "Studies of lithium intercalation into carbons using nonaqueous electrochemical cells," *Journal of The Electrochemical Society,* vol. 137, pp. 2009-2013, 1990.

[35] R. Yazami, "Surface chemistry and lithium storage capability of the graphite–lithium electrode," *Electrochimica acta,* vol. 45, pp. 87-97, 1999.

[36] M. Smart, B. Ratnakumar, L. Whitcanack, K. Chin, S. Surampudi, H. Croft, *et al.*, "Improved low-temperature performance of lithium-ion cells with quaternary carbonate-based electrolytes," *Journal of power sources,* vol. 119, pp. 349-358, 2003.

[37] V. Koch, L. Dominey, C. Nanjundiah, and M. Ondrechen, "The Intrinsic Anodic Stability of Several Anions Comprising Solvent-Free Ionic Liquids," *Journal of the Electrochemical Society,* vol. 143, pp. 798-803, 1996.

[38] Y. Wang, K. Zaghib, A. Guerfi, F. F. Bazito, R. M. Torresi, and J. Dahn, "Accelerating rate calorimetry studies of the reactions between ionic liquids and charged lithium ion battery electrode materials," *Electrochimica acta,* vol. 52, pp. 6346-6352, 2007.

[39] J. Bates, N. Dudney, B. Neudecker, A. Ueda, and C. Evans, "Thin-film lithium and lithium-ion batteries," *Solid State Ionics,* vol. 135, pp. 33-45, 2000.

[40] J. Trevey, J. S. Jang, Y. S. Jung, C. R. Stoldt, and S.-H. Lee, "Glass-ceramic Li_2S-P_2S_5 electrolytes prepared by a single step ball billing process and their application for all-solid-state lithium-ion batteries," *Electrochemistry communications,* vol. 11, pp. 1830-1833, 2009.

[41] A. Sakuda, H. Kitaura, A. Hayashi, K. Tadanaga, and M. Tatsumisago, "Improvement of high-rate performance of all-solid-state lithium secondary batteries using $LiCoO_2$ coated with Li_2O–SiO_2 glasses," *Electrochemical and Solid-State Letters,* vol. 11, pp. A1-A3, 2008.

[42] T. Minami, A. Hayashi, and M. Tatsumisago, "Recent progress of glass and glass-ceramics as solid electrolytes for lithium secondary batteries," *Solid State Ionics,* vol. 177, pp. 2715-2720, 2006.

[43] Y. Wang, Z. Liu, F. Huang, J. Yang, and J. Sun, "A Strategy to Improve the Overall Performance of the Lithium Ion-Conducting Solid Electrolyte $Li_{0.36}La_{0.56}0.08Ti_{0.97}Al_{0.03}O_3$," *European Journal of Inorganic Chemistry,* vol. 2008, pp. 5599-5602, 2008.

[44] Z. Liu, F. Huang, J. Yang, B. Wang, and J. Sun, "New lithium ion conductor, thio-LISICON lithium zirconium sulfide system," *Solid State Ionics,* vol. 179, pp. 1714-1716, 2008.

[45] J. Ibarra, A. Varez, C. León, J. Santamarıa, L. Torres-Martınez, and J. Sanz, "Influence of composition on the structure and conductivity of the fast ionic conductors $La_{2/3-x}\ Li_{3x}TiO_3$ ($0.03 \leq x \leq 0.167$)," *Solid State Ionics,* vol. 134, pp. 219-228, 2000.

[46] Y. Maruyama, H. Ogawa, M. Kamimura, S. Ono, and M. Kobayashi, "Dynamical properties and electronic structure of (LaLi) TiO_3 conductors," *Ionics,* vol. 14, pp. 357-361, 2008.

[47] O. Bohnke, "The fast lithium-ion conducting oxides $Li_{3x}\ La_{2/3-x}\ TiO_3$ from fundamentals to application," *Solid State Ionics,* vol. 179, pp. 9-15, 2008.

[48] R. Jimenez, A. Varez, and J. Sanz, "Influence of octahedral tilting and composition on electrical properties of the $Li_{0.2-x}\ Na_xLa_{0.6}TiO_3$ ($0 \leq x \leq 0.2$) series," *Solid State Ionics,* vol. 179, pp. 495-502, 2008.

[49] J. Percival, D. Apperley, and P. Slater, "Synthesis and structural characterisation of the Li ion conducting garnet-related systems, $Li_6\ ALa_2Nb_2O_{12}$ (A= Ca, Sr)," *Solid State Ionics,* vol. 179, pp. 1693-1696, 2008.

[50] Y. Zou, N. Inoue, K. Ohara, V. Thangaduri, and W. Weppner, "Structure and lithium ionic conduction of B-site Al-ion substitution in $La_{4/3}$-$yLi_{3y}Ti_2O_6$," *Ionics,* vol. 10, pp. 463-468, 2004.

[51] B. Kumar, D. Thomas, and J. Kumar, "Space-Charge-Mediated Superionic Transport in Lithium Ion Conducting Glass–Ceramics," *Journal of The Electrochemical Society,* vol. 156, pp. A506-A513, 2009.

[52] J. S. Thokchom and B. Kumar, "The effects of crystallization parameters on the ionic conductivity of a lithium aluminum germanium phosphate glass–ceramic," *Journal of Power Sources,* vol. 195, pp. 2870-2876, 2010.

[53] S. Hasegawa, N. Imanishi, T. Zhang, J. Xie, A. Hirano, Y. Takeda, *et al.*, "Study on lithium/air secondary batteries—Stability of NASICON-type lithium ion conducting glass–ceramics with water," *Journal of Power Sources,* vol. 189, pp. 371-377, 2009.

[54] M. Marzantowicz, J. Dygas, F. Krok, A. Tomaszewska, Z. Florjańczyk, E. Zygadło-Monikowska, *et al.*, "Star-branched poly (ethylene oxide) LiN $(CF_3SO_2)_2$: A promising polymer electrolyte," *Journal of Power Sources,* vol. 194, pp. 51-57, 2009.

[55] X. Yu, J. Bates, G. Jellison, and F. Hart, "A Stable Thin-Film Lithium Electrolyte: Lithium Phosphorus Oxynitride," *Journal of the electrochemical society,* vol. 144, pp. 524-532, 1997.

[56] K. Takada, T. Inada, A. Kajiyama, H. Sasaki, S. Kondo, M. Watanabe, *et al.*, "Solid-state lithium battery with graphite anode," *Solid State Ionics,* vol. 158, pp. 269-274, 2003.

[57] B. Bae, B.-H. Chun, and D. Kim, "Surface characterization of microporous polypropylene membranes modified by plasma treatment," *Polymer,* vol. 42, pp. 7879-7885, 2001.

[58] F. Laman, M. Gee, and J. Denovan, "Impedance studies for separators in rechargeable lithium batteries," *Journal of The Electrochemical Society,* vol. 140, pp. L51-L53, 1993.

[59] G. Venugopal, J. Moore, J. Howard, and S. Pendalwar, "Characterization of microporous separators for lithium-ion batteries," *Journal of power sources,* vol. 77, pp. 34-41, 1999.

[60] M. S. Whittingham, "The Role of Ternary Phases in Cathode Reactions," *Journal of The Electrochemical Society,* vol. 123, pp. 315-320, 1976 .

[61] A. Pan, J.-G. Zhang, Z. Nie, G. Cao, B. W. Arey, G. Li, *et al.*, "Facile synthesized nanorod structured vanadium pentoxide for high-rate lithium batteries," *Journal of Materials Chemistry,* vol. 20, pp. 9193-9199, 2010.

[62] C. Wu and Y. Xie, "Promising vanadium oxide and hydroxide nanostructures: from energy storage to energy saving," *Energy & Environmental Science,* vol. 3, pp. 1191-1206, 2010.

[63] J. M. Cocciantelli, J. P. Doumerc, M. Pouchard, M. Broussely, and J. Labat, "Crystal chemistry of electrochemically inserted $Li_xV_2O_5$," *Journal of Power Sources,* vol. 34, pp. 103-111, 1991.

[64] C. Delmas, S. Brèthes, and M. Ménétrier, "ω-$Li_xV_2O_5$ — a new electrode material for rechargeable lithium batteries," *Journal of Power Sources,* vol. 34, pp. 113-118, 1991.

[65] C. Cartier, A. Tranchant, M. Verdaguer, R. Messina, and H. Dexpert, "X-ray diffraction and X-ray absorption studies of the structural modifications induced by electrochemical lithium intercalation into V_2O_5," *Electrochimica Acta,* vol. 35, pp. 889-898, 1990.

[66] Y. Wang, K. Takahashi, K. H. Lee, and G. Z. Cao, "Nanostructured Vanadium Oxide Electrodes for Enhanced Lithium-Ion Intercalation," *Advanced Functional Materials,* vol. 16, pp. 1133-1144, 2006.

[67] D. Liu, Y. Liu, B. B. Garcia, Q. Zhang, A. Pan, Y.-H. Jeong, *et al.*, "V_2O_5 xerogel electrodes with much enhanced lithium-ion intercalation properties with N_2 annealing," *Journal of Materials Chemistry,* vol. 19, pp. 8789-8795, 2009.

[68] M. E. Spahr, P. Novák, W. Scheifele, O. Haas, and R. Nesper, "Electrochemistry of Chemically Lithiated NaV_3O_8: A Positive Electrode Material for Use in Rechargeable Lithium-Ion Batteries," *Journal of The Electrochemical Society,* vol. 145, pp. 421-427, 1998.

[69] Y. Xu, X. Han, L. Zheng, W. Yan, and Y. Xie, "Pillar effect on cyclability enhancement for aqueous lithium ion batteries: a new material of [small beta]-vanadium bronze $M_{0.33}V_2O_5$ (M = Ag, Na) nanowires," *Journal of Materials Chemistry,* vol. 21, pp. 14466-14472, 2011.

[70] I. D. Raistrick, "Lithium insertion reactions in tungsten and vanadium oxide bronzes," *Solid State Ionics,* vol. 9–10, Part 1, pp. 425-430, 1983.

[71] I. D. Raistrick and R. A. Huggins, "An electrochemical study of the mixed beta-vanadium bronzes $Li_yNa_xV_2O_5$ and $Li_yK_xV_2O_5$," *Materials Research Bulletin,* vol. 18, pp. 337-346, 1983.

[72] J. P. Pereira-Ramos, R. Messina, L. Znaidi, and N. Baffier, "Electrochemical lithium intercalation in $Na_{0.33}V_2O_5$ bronze prepared by sol-gel processes," *Solid State Ionics,* vol. 28–30, Part 1, pp. 886-894, 1988.

[73] S. Bach, J. P. Pereira-Ramos, N. Baffier, and R. Messina, "A Thermodynamic and Kinetic Study of Electrochemical Lithium Intercalation in $Na_{0.33}V_2O_5$ Bronze Prepared by a Sol-Gel Process," *Journal of The Electrochemical Society,* vol. 137, pp. 1042-1048, 1990.

[74] R. Baddour-Hadjean, S. Bach, N. Emery, and J. P. Pereira-Ramos, "The peculiar structural behaviour of [small beta]-$Na_{0.33}V_2O_5$ upon electrochemical lithium insertion," *Journal of Materials Chemistry,* vol. 21, pp. 11296-11305, 2011.

[75] E. Khoo, J. Wang, J. Ma, and P. S. Lee, "Electrochemical energy storage in a [small beta]-$Na_{0.33}V_2O_5$ nanobelt network and its application for supercapacitors," *Journal of Materials Chemistry,* vol. 20, pp. 8368-8374, 2010.

[76] H. Liu, Y. Wang, L. Li, K. Wang, E. Hosono, and H. Zhou, "Facile synthesis of NaV_6O_{15} nanorods and its electrochemical behavior as cathode material in rechargeable lithium batteries," *Journal of Materials Chemistry,* vol. 19, pp. 7885-7891, 2009.

[77] G. A. Wiegers, R. van der Meer, H. van Heiningen, H. J. Kloosterboer, and A. J. A. Alberink, "The sodium intercalates of vanadium disulfide and their hydrolysis products," *Materials Research Bulletin,* vol. 9, pp. 1261-1265, 1974.

[78] E. Lee, W. C. Lee, N. M. Asl, D. Kim, M. Slater, C. Johnson, *et al.*, "Reversible NaVS2 (De)Intercalation Cathode for Na-Ion Batteries," *ECS Electrochemistry Letters,* vol. 1, pp. A71-A73, 2012.

[79] Y. Kim and J. B. Goodenough, "Reinvestigation of $Li_{1-x}Ti_yV_{1-y}S_2$ Electrodes in Suitable Electrolyte: Highly Improved Electrochemical Properties," *Electrochemical and Solid-State Letters,* vol. 12, pp. A73-A75, 2009.

[80] A. R. Cooper and A. H. Heuer, *Mass transport phenomena in ceramics*: Plenum Press, 1975.

[81] X.-F. Zhang, K.-X. Wang, X. Wei, and J.-S. Chen, "Carbon-Coated V_2O_5 Nanocrystals as High Performance Cathode Material for Lithium Ion Batteries," *Chemistry of Materials,* vol. 23, pp. 5290-5292, 2011.

[82] W. Tang, X. Gao, Y. Zhu, Y. Yue, Y. Shi, Y. Wu, *et al.*, "A hybrid of V_2O_5 nanowires and MWCNTs coated with polypyrrole as an anode material for aqueous rechargeable lithium batteries with excellent cycling performance," *Journal of Materials Chemistry,* vol. 22, pp. 20143-20145, 2012.

[83] R. Baddour-Hadjean, J. Farcy, J. P. Pereira-Ramos, and N. Baffier, "A Kinetic Study of Lithium Transport in a New Li Intercalation Material $Al_{0.11}V_2O_{5.15}$ Synthesized via a Sol-Gel Process," *Journal of The Electrochemical Society,* vol. 143, pp. 2083-2088, 1996.

[84] J. Farcy, S. Maingot, P. Soudan, J. P. Pereira-Ramos, and N. Baffier, "Electrochemical properties of the mixed oxide $Fe_{0.11}V_2O_{5.16}$ as a Li intercalation compound," *Solid State Ionics,* vol. 99, pp. 61-69, 1997.

[85] P. Soudan, J. P. Pereira-Ramos, J. Farcy, G. Grégoire, and N. Baffier, "Sol-gel chromium–vanadium mixed oxides as lithium insertion compounds," *Solid State Ionics,* vol. 135, pp. 291-295, 2000.

[86] Y. Liu, X. Zhou, and Y. Guo, "Effects of fluorine doping on the electrochemical properties of LiV_3O_8 cathode material," *Electrochimica Acta,* vol. 54, pp. 3184-3190, 2009.

[87] M. D. Slater, D. Kim, E. Lee, and C. S. Johnson, "Sodium-Ion Batteries," *Advanced Functional Materials,* vol. 23, pp. 947-958, 2013.

[88] V. Palomares, P. Serras, I. Villaluenga, K. B. Hueso, J. Carretero-Gonzalez, and T. Rojo, "Na-ion batteries, recent advances and present challenges to become low cost energy storage systems," *Energy & Environmental Science,* vol. 5, pp. 5884-5901, 2012.

[89] A. Leblanc-Soreau, M. Danot, L. Trichet, and J. Rouxel, "Les intercalaires $A_xTi S_2$ et A_xZrS_2. Structure et liaisons. (A = Li, Na, K, Rb, Cs)," *Materials Research Bulletin,* vol. 9, pp. 191-197, 1974.

[90] K. M. Abraham, "Intercalation positive electrodes for rechargeable sodium cells," *Solid State Ionics,* vol. 7, pp. 199-212, 1982.

[91] D. Kim, S.-H. Kang, M. Slater, S. Rood, J. T. Vaughey, N. Karan, *et al.*, "Enabling Sodium Batteries Using Lithium-Substituted Sodium Layered Transition Metal Oxide Cathodes," *Advanced Energy Materials,* vol. 1, pp. 333-336, 2011.

[92] C. Didier, M. Guignard, C. Denage, O. Szajwaj, S. Ito, I. Saadoune, *et al.*, "Electrochemical Na-Deintercalation from $NaVO_2$," *Electrochemical and Solid-State Letters,* vol. 14, pp. A75-A78, 2011.

[93] C. S. Johnson, J.-S. Kim, A. J. Kropf, A. J. Kahaian, J. T. Vaughey, L. M. L. Fransson, *et al.*, "Structural Characterization of Layered $Li_xNi_{0.5}Mn_{0.5}O_2$ ($0 < x \leq 2$) Oxide Electrodes for Li Batteries," *Chemistry of Materials,* vol. 15, pp. 2313-2322, 2003.

[94] A. Le Bail, H. Duroy, and J. L. Fourquet, "Ab-initio structure determination of $LiSbWO_6$ by X-ray powder diffraction," *Materials Research Bulletin,* vol. 23, pp. 447-452, 1988.

[95] M. S. Whittingham, "Chemistry of intercalation compounds: Metal guests in chalcogenide hosts," *Progress in Solid State Chemistry,* vol. 12, pp. 41-99, 1978.

[96] B. Y. Liaw, I. D. Raistrick, and R. A. Huggins, "Thermodynamic and structural considerations of insertion reactions in lithium vanadium bronze structures," *Solid state ionics,* vol. 45, pp. 323-328, 1991.

[97] J. Galy, "Vanadium pentoxide and vanadium oxide bronzes—Structural chemistry of single (S) and double (D) layer $M_xV_2O_5$ phases," *Journal of Solid State Chemistry,* vol. 100, pp. 229-245, 1992.

[98] G. Yang, G. Wang, and W. Hou, "Microwave solid-state synthesis of LiV_3O_8 as cathode material for lithium batteries," *The Journal of Physical Chemistry B,* vol. 109, pp. 11186-11196, 2005.

[99] H.-g. Wang, D.-l. Ma, Y. Huang, and X.-b. Zhang, "Electrospun V_2O_5 Nanostructures with Controllable Morphology as High-Performance Cathode Materials for Lithium-Ion Batteries," *Chemistry – A European Journal,* vol. 18, pp. 8987-8993, 2012.

[100] D. Yu, C. Chen, S. Xie, Y. Liu, K. Park, X. Zhou, *et al.*, "Mesoporous vanadium pentoxide nanofibers with significantly enhanced Li-ion storage properties by electrospinning," *Energy & Environmental Science,* vol. 4, pp. 858-861, 2011.

[101] P. Ragupathy, S. Shivakumara, H. N. Vasan, and N. Munichandraiah, "Preparation of Nanostrip V_2O_5 by the Polyol Method and Its Electrochemical Characterization as Cathode Material for Rechargeable Lithium Batteries," *The Journal of Physical Chemistry C,* vol. 112, pp. 16700-16707, 2008.

[102] Y. L. Cheah, V. Aravindan, and S. Madhavi, "Electrochemical Lithium Insertion Behavior of Combustion Synthesized V_2O_5 Cathodes for Lithium-Ion Batteries," *Journal of The Electrochemical Society,* vol. 159, pp. A273-A280, 2012.

[103] X. Ren, Y. Jiang, P. Zhang, J. Liu, and Q. Zhang, "Preparation and electrochemical properties of V_2O_5 submicron-belts synthesized by a sol–gel H_2O_2 route," *Journal of Sol-Gel Science and Technology,* vol. 51, pp. 133-138, 2009.

[104] T. Zhai, H. Liu, H. Li, X. Fang, M. Liao, L. Li, *et al.*, "Centimeter-Long V_2O_5 Nanowires: From Synthesis to Field-Emission, Electrochemical, Electrical Transport, and Photoconductive Properties," *Advanced Materials,* vol. 22, pp. 2547-2552, 2010.

[105] Y. Chen, G. Yang, Z. Zhang, X. Yang, W. Hou, and J.-J. Zhu, "Polyaniline-intercalated layered vanadium oxide nanocomposites-One-pot hydrothermal synthesis and application in lithium battery," *Nanoscale,* vol. 2, pp. 2131-2138, 2010.

[106] S. Wang, Z. Lu, D. Wang, C. Li, C. Chen, and Y. Yin, "Porous monodisperse V_2O_5 microspheres as cathode materials for lithium-ion batteries," *Journal of Materials Chemistry,* vol. 21, pp. 6365-6369, 2011.

[107] G. Tchangbedji, D. A. Odink, and G. Ouvrard, "V_2O_4S — a new transition metal oxysulfide as positive for lithium batteries," *Journal of Power Sources,* vol. 44, pp. 577-581, 1993.

[108] G. Ouvrard, E. Prouzet, and G. Tchangbédji, "A New Soft Chemistry Synthesized Vanadium Oxysulfide," in *Materials Science Forum,* 1994, pp. 319-322.

[109] G. Ouvrard, G. Tchangbédji, P. Deniard, and E. Prouzet, "Structural, physical and electrochemical characteristics of a vanadium oxysulfide, a cathode material for lithium batteries," *Journal of Power Sources,* vol. 54, pp. 246-249, 1995.

[110] K. West, B. Zachau-Christiansen, S. Skaarup, Y. Saidi, J. Barker, I. I. Olsen, *et al.*, "Comparison of LiV_3O_8 Cathode Materials Prepared by Different Methods," *Journal of The Electrochemical Society,* vol. 143, pp. 820-825, 1996.

[111] C. Q. Feng, L. F. Huang, Z. P. Guo, J. Z. Wang, and H. K. Liu, "Synthesis and electrochemical properties of $LiY_{0.1}V_3O_8$," *Journal of Power Sources,* vol. 174, pp. 548-551, 2007.

[112] J. Jiang, Z. Wang, and L. Chen, "Structural and Electrochemical Studies on β-$Li_xV_2O_5$ as Cathode Material for Rechargeable Lithium Batteries," *The Journal of Physical Chemistry C,* vol. 111, pp. 10707-10711, 2007.

[113] P. Hagenmuller, *Comprehensive Inorganic Chemistry,* vol. 4, pp. 569-601, 1973.

[114] I. D. Raistrick and R. A. Huggins, "Electrochemical studies of lithium insertion reactions of vanadium oxide bronzes," 1984, pp. 374-384.

[115] R. Baddour-Hadjean, S. Bach, N. Emery, and J. P. Pereira-Ramos, "The peculiar structural behaviour of β-$Na_{0.33}V_2O_5$ upon electrochemical lithium insertion," *Journal of Materials Chemistry,* vol. 21, pp. 11296-11305, 2011.

[116] P. Cui, Z. Jia, L. Li, and T. He, "Study on the performance characteristics of Li–V–O nanocomposite as cathode material for Li-ion batteries," *Electrochimica Acta,* vol. 56, pp. 4571-4575, 2011.